



An Improved Model of Moderate Sleep Apnoea for Investigating Its Effect as a Comorbidity on Neurodegenerative Disease

Reno Roberts¹, Mark J. Wall¹, Ingke Braren², Karendeep Dhillon¹, Amy Evans¹, Jack Dunne¹, Simbarashe Nyakupinda¹ and Robert T. R. Huckstepp^{1*}

¹ School of Life Sciences, University of Warwick, Coventry, United Kingdom, ² University Medical Center Eppendorf, Vector Facility, Institute for Experimental Pharmacology and Toxicology, Hamburg, Germany

OPEN ACCESS

Edited by:

Charlene E. Gamaldo,
Johns Hopkins University,
United States

Reviewed by:

Kun-Ze Lee,
National Sun Yat-sen
University, Taiwan
Arash Tadjalli,
University of Florida, United States

*Correspondence:

Robert T. R. Huckstepp
r.huckstepp@warwick.ac.uk

Specialty section:

This article was submitted to
Neurocognitive Aging and Behavior,
a section of the journal
Frontiers in Aging Neuroscience

Received: 24 January 2022

Accepted: 19 April 2022

Published: 29 June 2022

Citation:

Roberts R, Wall MJ, Braren I,
Dhillon K, Evans A, Dunne J,
Nyakupinda S and Huckstepp RTR
(2022) An Improved Model of
Moderate Sleep Apnoea for
Investigating Its Effect as a
Comorbidity on Neurodegenerative
Disease.
Front. Aging Neurosci. 14:861344.
doi: 10.3389/fnagi.2022.861344

Sleep apnoea is a highly prevalent disease that often goes undetected and is associated with poor clinical prognosis, especially as it exacerbates many different disease states. However, most animal models of sleep apnoea (e.g., intermittent hypoxia) have recently been dispelled as physiologically unrealistic and are often unduly severe. Owing to a lack of appropriate models, little is known about the causative link between sleep apnoea and its comorbidities. To overcome these problems, we have created a more realistic animal model of moderate sleep apnoea by reducing the excitability of the respiratory network. This has been achieved through controlled genetically mediated lesions of the preBötzinger complex (preBötC), the inspiratory oscillator. This novel model shows increases in sleep disordered breathing with alterations in breathing during wakefulness (decreased frequency and increased tidal volume) as observed clinically. The increase in dyspnoeic episodes leads to reduction in REM sleep, with all lost active sleep being spent in the awake state. The increase in hypoxic and hypercapnic insults induces both systemic and neural inflammation. Alterations in neurophysiology, an inhibition of hippocampal long-term potentiation (LTP), is reflected in deficits in both long- and short-term spatial memory. This improved model of moderate sleep apnoea may be the key to understanding why this disorder has such far-reaching and often fatal effects on end-organ function.

Keywords: cognitive decline, sleep apnoea (SA), neuroinflammation, neurodegeneration, sleep deprivation (SD)

INTRODUCTION

Current estimates of the prevalence of moderate to severe (≥ 15 events.h⁻¹) sleep apnoea (SA, > 10 s of respiratory depression, ~ 2 missed breaths during sleep) are $\sim 4\%$ for men and $\sim 2\%$ for women in the United Kingdom (Young et al., 1993). However, recent large cohort studies show that 91% of SA cases are undetected (Tan et al., 2016), with an occurrence of $\sim 50\%$ of men and $\sim 25\%$ of women over 40 (Heinzer et al., 2015).

During rapid eye movement (REM) sleep, individuals experience increased upper airway resistance (Rowley et al., 1998) due to tonic motor inhibition lowering muscle tone (Xie, 2012). This increases vulnerability to repetitive pharyngeal collapse and cessation in airflow even in the presence of respiratory effort, otherwise known as obstructive sleep apnoea (OSA) (Remmers et al., 1978). During non-REM (NREM) sleep, loss of descending inputs in respiratory centers means control of breathing is solely modulated by metabolic factors, and breathing is more reliant on chemoreception (Xie, 2012). Thus, any defects in the respiratory microcircuit will be exposed, leading to loss of drive in respiratory muscles, termed central sleep apnoea (CSA) (Xie, 2012). Whilst it is believed that OSA is primarily a REM-related disorder with CSA occurring in NREM, both CSA and OSA can occur during either NREM or REM sleep (Loadsman and Wilcox, 2000; Gupta et al., 2016). In all cases, patients experience intermittent hypoxic hypercapnia following periods of apnoea (>90% reduction in ventilation) and hypopnoea (>50% reduction in ventilation) (Veasey and Rosen, 2019).

SA-related blood/gas changes induce oxidative imbalance, facilitating the generation and buildup of reactive oxygen species (ROS), leading to the development of systemic inflammatory-related biomarkers associated with chronic inflammation (Maniaci et al., 2021). Molecular markers of systemic inflammation are increased in patients with SA (McNicholas, 2009), elevating the risk of diseases with an underlying inflammatory component, e.g., cardiovascular disease (CVD) (Gottlieb et al., 2010), diabetes (Reutrakul and Mokhlesi, 2017), and dementia (Bahia and Pereira, 2015). Systemically, this can cause heart failure (HF) (Matuska et al., 2013), with mortality directly related to SA severity (Lanfranchi et al., 1999) and SA treatment decreasing mortality (Javaheri et al., 2011) and morbidity (Lavergne et al., 2015). SA causes endothelial dysfunction through inflammation, which is capable of impairing cerebral blood flow (Zuliani et al., 2008). In addition, an increase in hypertension (Calbet, 2003) and atherosclerosis (Drager et al., 2011) in SA patients elicits recurrent strokes (Brown et al., 2019). Furthermore, the hypercapnic hypoxia leads directly to oxidative stress and neuroinflammation (Dusak et al., 2013; Yang et al., 2013). All of these brain insults, individually or in combination, decrease hippocampal and grey matter volume (Dusak et al., 2013; Yang et al., 2013), resulting in memory deficits and cognitive decline (Yang et al., 2013; Bahia and Pereira, 2015).

Current animal models of SA used to study these pathways and associations are severely flawed: *chronic intermittent hypoxia* replicates the hypoxia observed during SA, but increased compensatory breathing leads to hypocapnia, the *opposite* of the clinical condition. Airway occlusion replicates the blood gas changes that occur during apnoea, but the frequency and duration of apnoeas *do not* replicate the clinical presentation. In both of these models, the simulated “apnoeas” continued after arousal or occur during wakefulness, initiating the defense response, which is physiologically *unrealistic* and will contribute to any related comorbidities. A recent model of SA used substance P, a neuromodulator that binds to neurokinin-1 receptors (NK1Rs) on neurones in the respiratory rhythm

generator, conjugated to saporin, a neurotoxin (SP-SAP) (Mckay and Feldman, 2008). Emulating this model, using a genetic approach via targeted viral transduction, we have developed an improved model of moderate SA that only displays apnoeas during natural sleeping patterns. Furthermore, our model displays both systemic and neural inflammation, inducing altered neuronal activity in the hippocampus and cognitive deficits. This novel model of moderate SA can be utilized for investigating the influence of SA on associated conditions such as neurodegenerative disease.

METHODS

Recombinant Adeno-Associated Virus (rAAV) Vector Particle Production and Purification

rAAVs were produced in Sf9 insect cells. rAAV transfer plasmids were derived from pFBGR (kindly provided by Robert Kotin, National Heart, Lung and Blood Institute, National Institutes of Health, Bethesda, MD, United States). Diphtheria toxin fragment A (DTA) followed by IRES and GFP as a fluorescent marker was inserted into pFBGR under the control of a human synapsin promoter by InFusion cloning. Two fragments were generated by PCR using PrimeStar GLX Polymerase (Clontech laboratories, Mountain View, CA, United States): the human synapsin promoter was amplified from pAAV-Syn-Venus (Tang et al., 2009) using 5'-tctagaatattaaggtacgggaggtacttgg and 5'-GATCcttgctagcagcttgaattcgactgcgctctca. DTA-IRES-GFP was amplified from pAAV-DTA-IRES-GFP (kindly donated by Prof. Alex Gourine, UCL) using 5'-ctgctagaacgATCaccATG GATCCTGATGATGTTGTTG and 5'-ggcgcaattgggtaccTTAC TTGTACAGCTCGTCCATGC. pFBGR was cut with MluI and KpnI, and both fragments were inserted simultaneously using the InFusion HD Cloning Kit (Clontech laboratories, Mountain View, CA, United States) according to the recommendations of the manufacturer to generate the AAV transfer plasmid pFBGR-Ultra Syn DTA-IRES-GFP. Final AAV transfer plasmids were confirmed by restriction digest, by PCR using the specific primers mentioned above, and by sequencing.

For packaging of AAV serotype 1 particles, pSR651 (Addgene plasmid 65213, addgene, Watertown, MA, United States) was employed. For packaging of AAV serotype 2 particles, pSR657 (Addgene plasmid 65214, addgene, Watertown, MA, United States) was employed (Smith et al., 2009). For producing rAAV serotype 9 particles, pFastBacDual (Life Technologies, CA, United States) was employed, and rep2 and cap9 were introduced (Chen, 2008).

To monitor Sf9 transduction efficiency during rAAV production, GFP was introduced into pFBGR under the control of a baculoviral late basic promoter (pB), and mCherry was introduced into pSR651 and pSR657, generating pFBGR-Ultra GFP and pSR651-Ultra mCherry and pSR657-Ultra mCherry (“Ultra-Bac,” Philipps et al., 2005). pB was amplified from Baculovirus Genomic DNA using 5'-GCAAT TGTTGTTGTTAAATTCCGTTTTGCGACGATGC and GTTAAATTGTGTAATTTATGTAGCTG. GFP was amplified

from pscAAV-GFP, and mCherry was amplified from pSicoR-Ef1a-mCh-Puro-GFPi (Addgene plasmid 31848, addgene, Watertown, MA, United States) using 5'-TTACACAATTTAAA CGtagcATGGTGAGCAAGGGCGAGG and 5'-tgcaataacaagtt aacTTACTTGTACAGCTCGTCCATGC.

Baculovirus genomic DNA carrying AAV genomic components and packaging elements was produced according to the Bac-to-Bac Expression System (Life Technologies, CA, United States) and according to the recommendations of the manufacturer. *E.coli* DH10Bac were transformed, and colonies were grown on kanamycin/tetracyclin/gentamycin plates supplemented with IPTG/Bluo-Gal. Large white colonies were propagated in 5 mL of 2YT medium containing kanamycin/tetracyclin/gentamycin overnight. Baculoviral DNA was extracted by Miniprep alkaline lysis, precipitated with 2-propanol, and resuspended in 50 μ L of ddH₂O. Clones were verified by PCR using Synapsin/T7 promoter specific primers.

rAAVs were produced according to "titreless infected-cell preservation and scale-up (TIPS)" protocol (Wasilko et al., 2009). Therefore, Sf9 cells were seeded on 12-well plates, and baculovirus DNAs derived from pFBGR-Ultra Syn DTA-IRES-GFP, pSR651-Ultra mCherry, pSR657-Ultra mCherry, and pFastBacDual-Ultra rep2 cap9 were transfected with the recombinant baculoviral genomic DNA using TransIT-Insect (MoBI Tec, Göttingen, Germany) according to the recommendations of the manufacturer. After 3 days, transfection could be monitored by mCherry or GFP fluorescence. Sf9 cells were collected, and 2E+07 fresh Sf9 cells were infected with this primary stock. After 1 day, vital fluorescing Sf9 cells were collected and frozen at 2E+6 cells BIIC stocks in InsectXpress/10% DMSO, also known as baculovirusinfected insect cells (BIIC).

For production of rAAV, ~4E+08 fresh Sf9 cells (Merck, NJ, United States) were cultivated in InsectXpress Medium (Lonza, Basel, Switzerland) at a density of 1–2E+6 cells·mL⁻¹; ~2E+06 Sf9 BIIC stocks containing the expression cassette Syn DTA-IRES-GFP and ~2E+06 Sf9 BIIC stocks containing the desired AAV packaging elements were added. After 4 days, cells were harvested and spun down for 20 min at 2,000 \times g. The cell pellet was resuspended in lysis buffer (50 mM Tris base, 100 mM NaCl, 5 mM MgCl₂, pH 8.5), and viral particles were released from the nucleus by three freeze-thaw cycles. Any virus released into the supernatant was precipitated by incubation overnight in 10% PEG-8000/1 M NaCl at 4°C and then centrifuged for 30 min at 4°C and 3,000 \times g. The resulting pellet was resuspended in lysis buffer and combined with cell lysate. Benzonase (Merck KGaA, Darmstadt, Germany; final concentration 50 U·mL⁻¹) was added and incubated for 1 h at 37°C. Cell debris was pelleted for 20 min at 12,000 \times g and vector containing lysates were purified using iodixanol step gradients. Iodixanol 40% layers were harvested, and iodixanol was removed by ultrafiltration (Amicon Ultra-4 Centrifugal Filter Unit, 50-kDa cutoff; Millipore, Burlington, MA, United States).

The genomic titres of DNase-resistant recombinant AAV6 particles were determined by quantitative PCR using SYBR Green qPCR Master MIX 2 (Thermo Fisher Scientific, Waltham, MA, United States) and an ABI 7900 HT cycler (ABI, Waltham,

MA, United States). Viral vectors were quantified using T7/SV40 specific primers (5'-cctatagtagtgcgtattacgcgc and 5'-gctgcaataacaagttggccat).

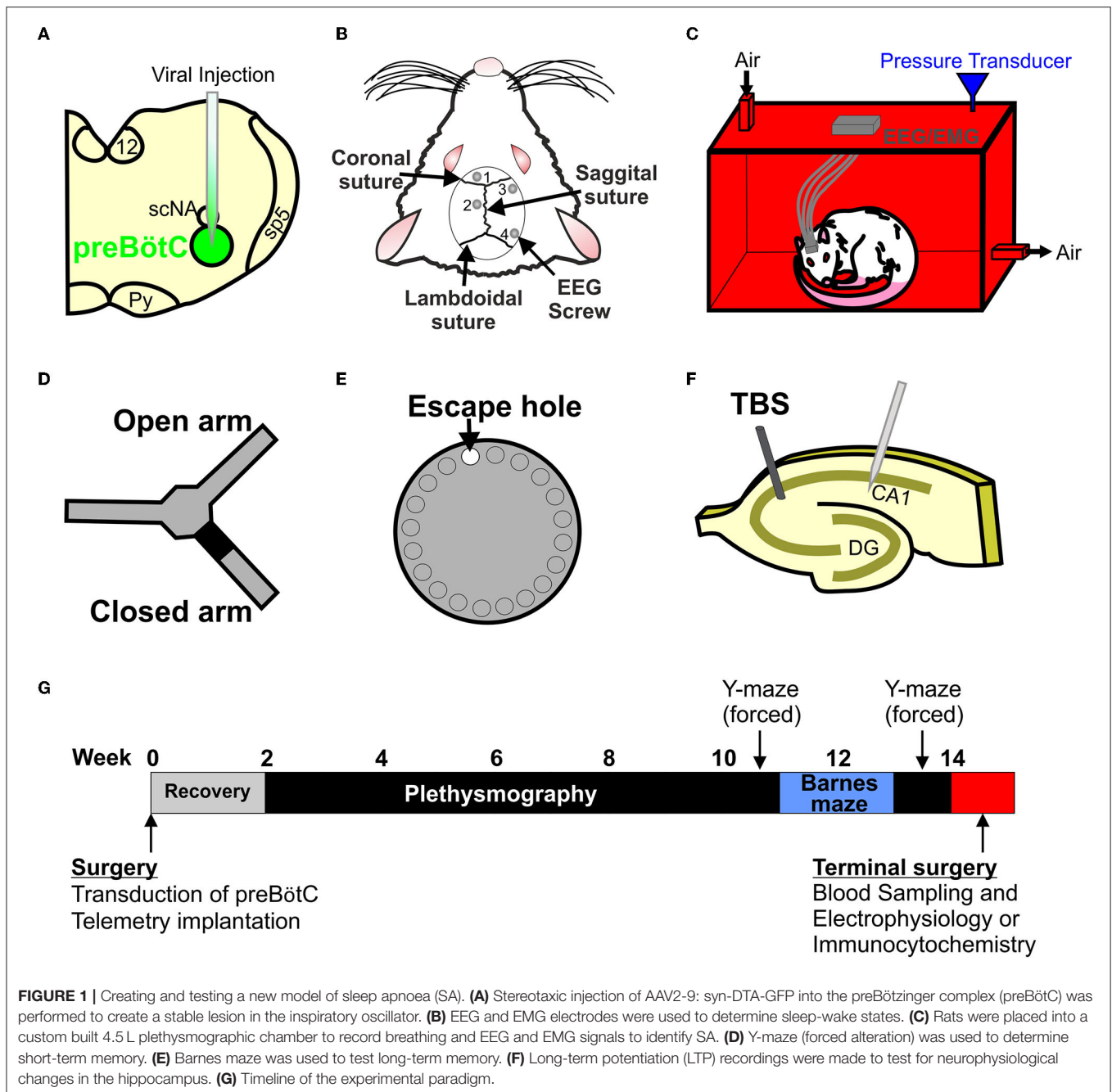
Real-time PCR was conducted at 10 μ L with 0.3 μ M for each primer. Fluorescence was measured at the end of each annealing phase. AAV transfer plasmids were employed as a copy number standard. A standard curve for quantification was generated by serial dilutions of the respective vector plasmid DNA. The cycling conditions were as follows: 50°C for 2 min, 95°C for 10 min, followed by 35 cycles of 95°C for 15 s and 60°C for 60 s. Calculations were performed using the SDS 2.4 software (ABI, Waltham, MA, United States).

Virus Handling

AAV2-9: syn-DTA-GFP (AAV:syn-DTA) at a titer of 3.87×10^{13} VP·mL⁻¹ was aliquoted and stored at -80°C. On the day of injection, viruses were removed and held at 4°C, loaded into graduated glass pipettes (Drummond Scientific Company, Broomall, PA, United States), which were placed into a pipette holder for pressure injection. The AAV:syn-DTA used the synapsin promoter, transducing neurones with higher tropism for the AAV2-9 subtype; it did not transduce non-neuronal cells.

Viral Transduction of preBötC Neurones

Adult male Sprague Dawley rats, between 6–8 months of age, were pseudorandomized by order and surgery type. Sham-operated rats weighed 437 ± 82 g ($n = 17$), whilst DTA-injected rats weighed 456 ± 61 g ($n = 11$). Three animals were excluded because of cortical brain injury caused by placement of EEG electrodes. Rats were anesthetized via intramuscular injection with ketamine (100 mg·kg⁻¹; Covetrus, Dumfries, United Kingdom) and medetomidine (250 μ g·kg⁻¹; Covetrus, Dumfries, United Kingdom). Adequate anesthesia was maintained with 0.5–2% isoflurane (Piramal Healthcare, Mumbai, India) in pure oxygen (1 L·min⁻¹) throughout the surgery as required. Rats received a presurgical subcutaneous injection of atropine (120 μ g·kg⁻¹; Westward Pharmaceutical Co., Eatontown, NJ, United States) and meloxicam (2 mg·kg⁻¹; Norbrook Inc., Lenexa, KS, United States). Rats were placed prone into a digital stereotaxic apparatus (Kopf Instruments, Tujunga, CA, United States) on a heating pad (TCAT 2-LV: Physitemp, Clifton, NJ, United States), and body temperature was maintained at a minimum of 33°C via a thermocouple; mild hypothermia during surgery reduced blood loss and significantly improved post-surgical recovery. The head was angled so the nose bar was -18 mm below the intra-aural line. The injection arm was angled at 23°. Graduated glass pipettes containing the virus were placed stereotaxically into the preBötC (**Figure 1A**). The preBötC was defined as the area ventral to the semi-compact nucleus ambiguus (NA; coordinates: ± 1.95 mm lateral, -0.2 mm rostral and +0.4 mm caudal, and -2.95 mm ventral from the obex; **Figure 1A**). The virus solution was pressure injected (~300 nL per site) bilaterally into all 4 sites to ensure good coverage of the preBötC. Pipettes were left in place for 3–5 min to prevent backflow of virus solution up the pipette track. Postoperatively, rats received subcutaneous injections of buprenorphine (100 μ g·kg⁻¹; Reckitt Benckiser, Slough,



United Kingdom) and atipamezole ($1 \text{ mg}\cdot\text{kg}^{-1}$; Vetoquinol, Northamptonshire, United Kingdom).

Control Surgeries

Given the nature of the model, two separate controls were performed to account for different potential confounding factors.

Given 1 molecule of DTA is all that is required to induce apoptosis (Yamaizumi et al., 1978), any cell that expresses the plasmid undergoes apoptosis. Neurones of the preBötC of DTA-transduced rats are healthy and plasmid-free; we found no

expression of GFP in transduced cells from injected rats ($n = 4$). For our sham surgeries, pipettes were lowered 2 mm dorsoventral from the obex, with the same mediolateral and rostral coordinates. These rats will have been exposed to all of the same surgical procedures, but without any damage to the preBötC; allowing us to compare preBötCs containing a reduced number of healthy cells following DTA induced cell death in transduced rats with intact preBötCs in sham operated animals.

Preliminary experiments were conducted to determine injection number and volume. Injection volumes that did not

cause SA were used as a control group. Rats were injected with ~300 nL of AAV:syn-DTA either unilaterally in the aforementioned rostral and caudal coordinates or bilaterally in the aforementioned rostral coordinates. Rats that only received two injections of virus, be it unilaterally or bilaterally, did not display any signs of SA. Given these rats will have experienced cell death in the preBötC and will have released DTA into the extracellular milieu there, these rats act as control for the presence of apoptosis and the DTA subunit. As these rats showed no increase in AHI compared to sham-operated rats, data from the two controls were pooled. Therefore, we controlled for a change in preBötC size from wild-type levels, where all remaining neurones in both groups are free from viral transduction, and we also controlled for apoptosis and DTA production within the preBötC.

EEG and EMG Placement

Following viral injections, the head was leveled so the nose bar was set to 0 at the intraural line. Burr holes were drilled at 4 locations: (1) immediately rostral to the coronal suture in a mediolateral position central to the frontal bone plate on the left of the sagittal suture to the most lateral extent of the bone; (2) in a rostrocaudal position centered between the coronal and lambdoidal sutures in a central position on the left parietal bone plate between the sagittal suture and the most lateral extent of the bone; (3) immediately caudal to the coronal suture in a position on the right parietal bone plate centered between the sagittal suture and the most lateral extent of the bone; (4) immediately rostral to the lambdoidal suture in a position on the right parietal bone plate centered between the sagittal suture and the most lateral extent of the bone (**Figure 1B**). EMGs were placed bilaterally into the trapezius muscles. EEG electrodes (M1.4 × 3 mm Phillips Pan Head Machine Screws (DIN 7985H)—Stainless Steel (A2), SIP—M1.4-3-A2; Accu, Huddersfield, United Kingdom) and EMG wires were connected to custom-built headmounts. Headmounts were adhered to the skull with superbond dental cement (Prestige Dental, Bedworth, United Kingdom), with additional support from Vertex Orthoplast cold-curing orthodontic acrylic resin (Prestige Dental, Bedworth, United Kingdom). Rats were allowed 2 weeks to recover from surgery and for viral expression, with food and water *ad libitum* at an ambient temperature of $22 \pm 2^\circ\text{C}$. Following recovery, experimenters were blinded to the condition of the rats.

Plethysmography

The order of the rats was pseudorandomized each week. Rats were acclimated for 30 min to the chamber in their home cage. On a separate occasion, rats were acclimated to the plethysmography room with a 30 min recording session under experimental conditions in postsurgical week 2. Following acclimation, rats were recorded for a single 3 h session per week with the recordings continuing for 7 weeks between postsurgical weeks 3 and 9. Recordings were conducted during the light phase of the 12 h light/dark cycle. For recordings, rats were placed into a custom-built 4.5 L plethysmography chamber (**Figure 1C**), with an airflow rate of $2 \text{ L}\cdot\text{min}^{-1}$ and an average

temperature of $23 \pm 0.9^\circ\text{C}$; thermoneutral for rats housed at an ambient temperature of $22 \pm 2^\circ\text{C}$ (Poole and Stephenson, 1977). Rats did not show any sign of thermoregulation, e.g., panting, shivering, or hyper-locomotion, and they displayed normal sleeping patterns. Pressure transducer signals were amplified and filtered using the NeuroLog system connected to a 1401 interface (Digitimer, Welwyn Garden City, United Kingdom). All data were acquired on a computer using Spike2 software (Cambridge Electronic Design, Cambridge, United Kingdom). For our analysis, respiratory disturbances were defined as a reduction in minute ventilation by $>50\%$ (hypopnoea) or $>90\%$ (apnoea) for $\geq 1.8 \text{ s}$. This duration was selected as:

1. In humans, sleep-disordered breathing is defined as perturbed breathing for $\geq 10 \text{ s}$, which is ~ 2 breaths. In our experiments, rat respiratory rate was $105 \text{ breaths}\cdot\text{min}^{-1}$, or 2 breaths every 1.2 s. To ensure that we did not overestimate the severity of our model, we use a duration equivalent to 3 breaths.
2. Adult rats exposed to obstructive apnoeas $>5 \text{ s}$ in duration, display extreme O_2 desaturations in all events (Farré et al., 2007). Using the equation of the line from values for 10 and 15 s apnoeas from Farré et al. (2007), which predicts a resting saturation of 99%, we extrapolated the point at which apnoeas would reach an oxygen desaturation of 4% as $\sim 1.875 \text{ s}$.

Apnoeas and hypopnoeas were scored by hand, and the length of each event recorded. Respiratory parameters were measured during quiet wakefulness at the beginning of the recording. Airflow measurements were used to calculate: tidal volume (V_T), signal trough at the end of expiration subtracted from the peak signal during inspiration, converted to mL following calibration, and standardized to body weight; respiratory frequency (f) calculated as breaths per minute using peak of inspiration to peak of inspiration averaged over 1 min. Minute ventilation (V_E) was calculated as $V_T \times f$.

Sleep-Wake Recordings

Theta rhythms were obtained by differential recordings from electrodes 1 and 2 (see EEG and EMG Placement) positioned in the dorsal hippocampus and the frontal cortex, respectively (**Figure 1B**). Delta waves and neocortical EEG activity were obtained by differential recordings from electrodes 3 and 4 (**Figure 1B**). EEG signals were amplified 7,500-fold and bandpass-filtered at 5–70 Hz. EMG signals were recorded by differential recordings through the trapezoid wires (**Figure 1B**) and were amplified 4,500-fold and bandpass filtered at 50–1,500 Hz. Videos were recorded to aid with sleep-wake scoring. All data were acquired on a computer using Spike2 software. EEG and EMG signals were processed using the OSD4 script: EEGs were band-filtered with a power spectrum of 0–4 Hz (delta) and 6–10 Hz (theta), and smoothed with a 5 s time constant. EMGs were processed with a 5 s RMS time constant. The 3 h long recordings were separated in 5 s epochs. Sleep-wake scored epochs were categorized into 4 predefined classes: (1) WAKE: low-amplitude desynchronized EEG activity and high EMG power; (2) NREM: high-amplitude EEG delta waves and low EMG power; (3) REM: continuous low-amplitude EEG theta activity leading to high theta:delta (T:D) ratio, and no EMG

power, muscular paralysis could be observed on the associated video; (4) DOUBT: epochs that could not be defined into the 3 previous categories. For consistency, AHI counts and duration are expressed as per hour of total sleep even when discussing specific sleep states. Sigh counts are expressed as per hour of sleep + quiet wakefulness.

Barnes Maze

The Barnes maze is a 122-cm diameter circular maze with 20 holes: 19 false holes and one escape hole, all measuring 9 cm in diameter (Stoelting, Dublin, Ireland) (**Figure 1D**). The maze is 1 m off the ground. Spatial cues of different colours and shapes are spaced evenly around the maze at regular intervals in plain sight of the rats. The surface of the table is brightly lit (>1,500 lux) to create an adverse environment. The Barnes maze began on post-surgical week 10 with the order of the rats pseudorandomized before each session. Rats underwent a 12 day Barnes maze protocol: days 1–3 (learning phase): the escape hole (randomly assigned on day 1) contained an incentive (peanut butter); days 4–12 (acquisition phase): the incentive is provided in the home cage after the test, allowing the rats to be rewarded for completing the test but removing the olfactory stimulus from the maze. The task was completed when the rats' entire body entered the exit hole. For consistency between rats, behavioural and respiratory measurements were not taken on the same day, as plethysmography may affect Barnes maze performance. All runs were recorded using a camera system (Henelec Model 335 BWL; Sony, Surry, United Kingdom) attached to a computer for offline analysis (Any-MAZE v4.96; Stoelting, Dublin, Ireland). Total distance, duration, and exit errors were measured. Exit errors were counted as the number of times the rats visited the exit hole but remained on the maze. Heat maps of the rats' movements were created for determination of search strategy. These were: random, no consistent pattern with ≥ 2 crossings of the open field; serial, hole-by-hole progression with ≥ 3 consecutive holes visited; spatial, moving directly to within 2 holes of the exit hole and no deviation outside of the quadrant (Wall et al., 2018).

Y Maze (Forced Alternation)

A spontaneous spatial novelty preference test was conducted using a radial arm maze (Stoelting, Dublin, Ireland), adapted into a Y-maze. Each arm was 50 cm long and 10 cm wide, with 13-cm-high walls (**Figure 1E**). The surface of the table was comfortably lit (150–250 lux), with lighting levels consistent across the maze. Spatial cues of different colours and shapes were placed at the end of each arm of the maze. The order of the rats was pseudorandomized before each session. All rats were placed into the same entry arm. For the first trial, one arm of the Y-maze was blocked according to a pseudorandom sequence; therefore, rats could either go down to the unblocked arm, entry arm, or central region. First trials lasted for 10 min. After 1 h, the rats underwent the second trial to assess short-term memory. The second trial was performed with access to all arms. The Y maze took place either before or after the Barnes maze (week 10 or week 13). The order of the Barnes maze and Y-maze was determined by pseudorandomization during the experimental planning phase. All runs were recorded

using a camera system (Henelec Model 335 BWL; Sony Surry, United Kingdom) attached to a computer for offline analysis (Any-MAZE v4.96, Stoelting, Dublin, Ireland). Total distance, duration, and number of entries into each arm were measured. An entry into an arm was defined as placement of 2 paws into that arm.

Immunology

Rats were anesthetized by inhalation of isoflurane (0.5–2%; Piramal Healthcare, Mumbai, India) in room air (1 L·min⁻¹). Inferior vena cava blood samples were taken and placed on ice in a tube containing EDTA (1.5 mg·mL⁻¹ final concentration in the sample). Samples were spun at 13,000 rpm at 4°C for 10 min, and plasma was collected. Samples were aliquoted and stored at –80°C. Samples underwent no more than 2 freezing cycles.

Plasma samples were chosen as the relative differences between cytokines in serum and plasma would not be expected to be different. However, cellular components such as platelets can synthesize and release cytokines (Chen et al., 2020), which contribute to the overall amount of cytokines in serum. Therefore, plasma is considered to be a better reflection of circulating or any humoral cytokines when measured by enzyme-linked immunosorbent assay (ELISA).

Plasma samples were run on rat inflammation calorimetric sandwich ELISA kits (EA-1201 Signosis, Santa Clara, CA, United States) testing 8 inflammatory cytokines (TNF α , IL-6, MCP-1, IFN γ , RANTES, MIP, IL-1a, and IL-1b) and rat noradrenaline whole antibody sandwich ELISA kits (CSB-E07022R Cusabio, Houston, TX, United States). Optical densities were converted to concentrations via standard curves using protein standards (EA-1202 Signosis, Santa Clara, CA, United States). As a consequence of the variability in ELISA kits, measurements that did not lie on the linear part of the curve were discarded, and samples were run again. To further reduce the impact of the variability of ELISA kits, samples were pseudorandomized to kits and run in duplicate on different kits, with the exception of noradrenaline, which was measured using a single kit.

Collection of Brain Tissue

Rats were humanely killed by overdose of inhalation of isoflurane and decapitated with a guillotine. Brains were rapidly removed. The medulla and one cortical hemisphere were placed in 4% paraformaldehyde (PFA) for immunocytochemistry. The other cortical hemisphere was placed in ice cold saline for electrophysiological studies.

Immunocytochemistry

Brains were postfixed overnight in PFA (4°C) and cryoprotected in 30% sucrose. Brainstems and hippocampi were serially sectioned at 40 μ m. Free-floating sections were placed in a blocking solution (phosphate buffered saline [PBS] + 5% bovine serum albumin + 0.1% Triton X-100) and incubated for 1 h. Slices were further incubated overnight in blocking solution and primary antibodies: Medulla, rabbit anti-substance *p* receptor—(1:500; ab5060, Merck Millipore, Watford, United Kingdom) and mouse anti-NeuN (1:100; MAB337, Merck Millipore, Watford, United Kingdom) antibody; Hippocampus, goat anti-Iba1 (1:83;

ab5076, Abcam, Cambridge, United Kingdom) antibody. Slices were washed in blocking solution (6×5 min) and then incubated for 2–4 h in blocking solution containing secondary antibodies: Medulla, donkey anti-rabbit Alexa Fluor 568 (1:250; ab150074, Abcam, Cambridge, United Kingdom) or donkey anti-mouse Alexa Fluor 568 (1:250; A10037, Invitrogen, Waltham, MA, United States) antibody; Hippocampus, donkey anti-goat Alexa Fluor 488 (1:250; A11055, Invitrogen, Waltham, MA, United States). Slices were washed in PBS (6×5 min), mounted (Medulla: Cytoseal 60; Electron Microscopy Sciences, Hatfield, PA, United States. Hippocampus: Vectashield Antifade Mounting Medium with DAPI; Vectorlabs, Burlingame, CA, United States) and coverslipped.

The NK1R antibody has been used in 24 peer-reviewed publications and has been validated elsewhere. NK1R is present in the nucleus ambiguus, and staining of the compact and semi-compact ambiguus were observed acting as a positive control. NK1R staining was also absent from areas devoid of NK1R, such as the SP-5 tract (data not shown), providing a negative control. Given the pattern of staining, previous validation, and use of the antibody elsewhere, the NK1R antibody is specific for the NK1R. The NeuN antibody has been used in 1,085 peer-reviewed publications and has been extensively validated. NeuN staining appears to be nuclear, given size and shape, and was located in voids left by NK1R staining, which cannot penetrate the nucleus, acting as a positive control. NeuN staining was absent from areas devoid of neurones, such as the SP-5 tract (data not shown), providing a negative control. Given the pattern of staining, previous validation, and use of the antibody elsewhere, we are certain that the NeuN antibody is specific for the nuclei of neurones. The Iba1 antibody we selected has been used in 24 peer-reviewed publications and has been validated elsewhere. Cells expressing Iba1 staining have the distinctive shape of microglia, providing a positive control. Iba1 staining was largely absent from the wild-type tissue, which should be devoid of activated microglia, providing a negative control. Given the pattern of staining, previous validation, and use of the antibody elsewhere, we are certain that the Iba1 antibody is specific for activated microglia.

Slices were examined using a confocal fluorescent microscope (Zeiss 880; Zeiss, Jena, Germany) with Zen black and Zen blue software. For the medulla: to determine the efficacy of viral transduction, counts of NeuN positive cells were performed in representative 40- μ m sections throughout transduced brainstems and within a 600- μ m diameter circle below the semi-compact nucleus ambiguus (Mckay and Feldman, 2008). To establish loss of rhythm-generating preBötC neurones, following background subtraction, fluorescence intensity of NK1R staining was assessed in ImageJ within the same circle. For the hippocampus: to identify activated microglia, we counted DAPI-stained nuclei encapsulated with Iba1 anywhere in the visual field. This provided several advantages over the use of Iba1 alone. First, as we only stained every second slice, nuclei could only be present in a single slice, removing any possibility of overestimation by double counting. Iba1 staining around the nucleus is very distinct from the staining of the

processes, allowing us to distinguish nuclei enveloped in Iba1 from nuclei that have Iba1-positive projections in close apposition to them. These differences are amplified by imaging a z-stack with a confocal microscope when compared to standard fluorescence microscopy.

Extracellular Recording of *f*EPSPs in Hippocampal Slices

The order of the rats was pseudorandomized before LTP experiments began. 400- μ m thick sagittal slices of the hippocampus and overlying cortex were prepared under standard conditions in ice-cold aCSF (124 mM NaCl, 3 mM KCl, 2 mM CaCl₂, 26 mM NaHCO₃, 1.25 mM NaH₂PO₄, 1 mM MgSO₄, 10 mM D-glucose saturated with 95% O₂-5% CO₂, pH 7.5, containing an additional 10 mM MgCl₂). Slices were transferred to an incubation chamber containing aCSF at $32 \pm 1^\circ\text{C}$ and incubated for 1 h. All tissue slices were made at 9 am in the morning to standardize the amount of time rats had to sleep prior to removal of tissue. Extracellular recordings of synaptic transmission and plasticity were carried out using two recording rigs to increase productivity. Data from the two rigs were not statistically different and so were pooled.

Recording on rig 1: Slices were transferred to the recording chamber submerged in aCSF (124 mM NaCl, 3 mM KCl, 2 mM CaCl₂, 26 mM NaHCO₃, 1.25 mM NaH₂PO₄, 1 mM MgSO₄, and 10 mM D-glucose saturated with 95% O₂-5% CO₂; pH 7.5) and perfused at 4–6 mL·min⁻¹ (32°C). Slices were placed on a grid allowing perfusion above and below the tissue, and all tubing (Tygon, Akron, OH, United States) was gas-tight (to prevent loss of oxygen). To record field excitatory postsynaptic potentials (*f*EPSPs), an aCSF-filled microelectrode was placed on the surface of the stratum radiatum in CA1 (**Figure 1F**). A bipolar concentric stimulating electrode (CBBPC75, FHC, Bowdoin, ME, United States) controlled by an isolated pulse stimulator model (2100, AM Systems, WA, United States) was used to evoke *f*EPSPs in the Schaffer collateral–commissural pathway (**Figure 1F**). Field *f*EPSPs were evoked every 30 s (0.03 Hz). Stimulus input/output (I/O) curves for *f*EPSPs were generated using 0.5 V steps between 1 and 5 V for slices (stimulus duration 0.2 ms). Paired-pulse ratio was measured over intervals ranging between 20 to 500 ms (ratio averaged for 5 repeats at each interval). For synaptic plasticity experiments, stimulus strength was set to produce an *f*EPSP slope $\sim 40\%$ of the maximum response. Long-term potentiation (LTP) was induced by theta burst stimulation (TBS, 3 trains separated by 20 s, with a train consisting of 10 bursts of 4 pulses at 100 Hz, separated by 200 ms). Signals were filtered at 3 kHz and digitized online (10 kHz) with a Micro CED (Mark 2) interface controlled with Spike 2 software (Vs 6.1, Cambridge Electronic Design, Cambridge United Kingdom). The *f*EPSP slope was measured from a 1 ms linear region following the fiber volley. All I/O curves and PPF comparisons were made from this recording rig.

Recording on rig 2: *f*EPSPs were recorded as outlined for rig 1, except perfusion was set at 6–7 mL·min⁻¹. A bipolar concentric stimulating electrode (CBBPC75, FHC, Bowdoin, ME, United States) was controlled by a DS3 isolated current

stimulator (Digitimer, Welwyn Garden City, United Kingdom) with field *f*EPSPs evoked every 45 s. Stimulus input/output curves for *f*EPSPs were generated using 20- μ A steps between 20 and 300 μ A (stimulus duration 0.2 ms), stimulus strength was set to produce an *f*EPSP slope \sim 40 % of maximum response. Long-term potentiation was induced by theta burst stimulation (as above for rig 1). Signals were acquired using the WinLTP software (Vs 2.3; WinLTP Ltd., Bristol, United Kingdom).

Experimental Design

For transduction, the order of rats, and experimental type (whether they received viral injections or were shams) were pseudorandomized. Experimenters were blinded to the condition of the rats. Rats were acclimated to the plethysmography chamber for 30 min during the 2nd week post-surgery. Plethysmography began during the 3rd week post-surgery and continued for 7 weeks. Rats then underwent 1 day of Y-maze, 12 days of Barnes maze, and the order of maze testing was pseudo randomized for each batch. Tissue collection and LTP experiments were performed one week after the final maze session. Experimenters were unblinded to the condition of the rats once analysis had been performed (Figure 1G).

Control rats that received only 2 injections were acclimated to the plethysmography chamber on the 2nd week post-surgery. Plethysmography began on the 3rd week post-surgery and continued for 6 weeks. Tissue collection was performed one week after the final plethysmography session.

Data Analysis

All experimental units are an animal; all technical repeats are averaged to create a biological repeat for analysis. Outliers were removed after Iglewicz and Hoaglin's robust test for multiple outliers with an outlier criterion: modified Z score \geq 3.5 (<https://contchart.com/outliers.aspx>) or Grubb's test (OriginLab, Northampton, MA, United States). Shapiro-Wilk tests were performed on sham-operated groups.

Data for preBötC cell counts ($p = 0.5$), NA cell counts ($p = 0.8$), BötC cell counts ($p = 0.5$), preBötC corona cell counts ($p = 0.4$), preBötC NK1R intensity ($p = 0.08$), AHI ($p = 0.3$), time spent in disordered breathing ($p = 0.25$), AHI by sleep state (DTA: $p = 0.6$; sham: $p = 0.6$), time spent in disordered breathing by sleep state (DTA: $p = 0.5$; sham: $p = 0.5$), V_T ($p = 0.3$), f ($p = 0.1$), V_E ($p = 0.2$), WAKE ($p = 0.2$), NREM ($p = 0.1$), REM ($p = 0.4$), Iba1 counts ($p = 0.6$), IFN γ ($p = 0.06$), IL-1a ($p = 0.96$), IL-1b ($p = 0.4$) and IL-6 ($p = 0.3$), CRP ($p = 0.9$), noradrenaline ($p = 0.7$), and Y-maze discrimination ratios (duration: $p = 0.7$; distance: $p = 0.8$) were deemed Gaussian by a Shapiro-Wilk test for normality and tested by an unpaired *t*-test. The data are expressed as mean \pm SD.

Data for Barnes maze search strategies ($p = 0.2$) were deemed Gaussian by a Shapiro-Wilk test for normality and tested by a one-way repeated measures ANOVA with Bonferroni correction. The data are expressed as mean \pm SD.

Data for Y-maze novel arm entries ($p = 0.6$), Y-maze novel duration ($p = 0.98$), Y-maze novel arm distance ($p = 0.06$),

and paired pulse facilitation ($p = 0.6$) were deemed Gaussian by a Shapiro-Wilk test for normality and tested by a two-way repeated measures ANOVA with Bonferroni correction. The data are expressed as mean \pm SD.

Data for the average duration of apnoeas during sleep state (NREM: $p = 0.3$) and sleep state (REM: $p = 0.9$), were deemed Gaussian by a Shapiro-Wilk test for normality and tested by a two-way ANOVA. The data are expressed as mean \pm SD.

Data for CA1 Iba1 counts ($p = 0.02$), TNF α ($p = 0.02$), MCP-1 ($p = 0.03$), MIP ($p = 0.01$), RANTES (0.02), and Y-maze discrimination ratio for entries ($p = 0.001$) were deemed non-Gaussian by a Shapiro-Wilk test for normality and tested by a Kruskal-Wallis Test; 68% of the data are contained within 1 SD, and to make the data comparable, we calculated the data range from the 15th to 85th percentile, herein known as R₇₀. Data are expressed as median followed by the R₇₀ and displayed graphically as median with percentiles 15–85.

Data for Barnes duration ($p = 0$), Barnes maze distance ($p = 0$), Barnes maze exit errors ($p = 0$), and LTP ($p = 0.0002$) were deemed non-Gaussian by a Shapiro-Wilk test for normality and tested by a two-way repeated measures ANOVA with Sidak correction. The data are expressed as mean \pm SD.

Data for input-output curves ($p = 0.00005$) were deemed non-Gaussian by a Shapiro-Wilk test for normality and tested by a two-way ANOVA with Sidak correction. The data are expressed as mean \pm SD.

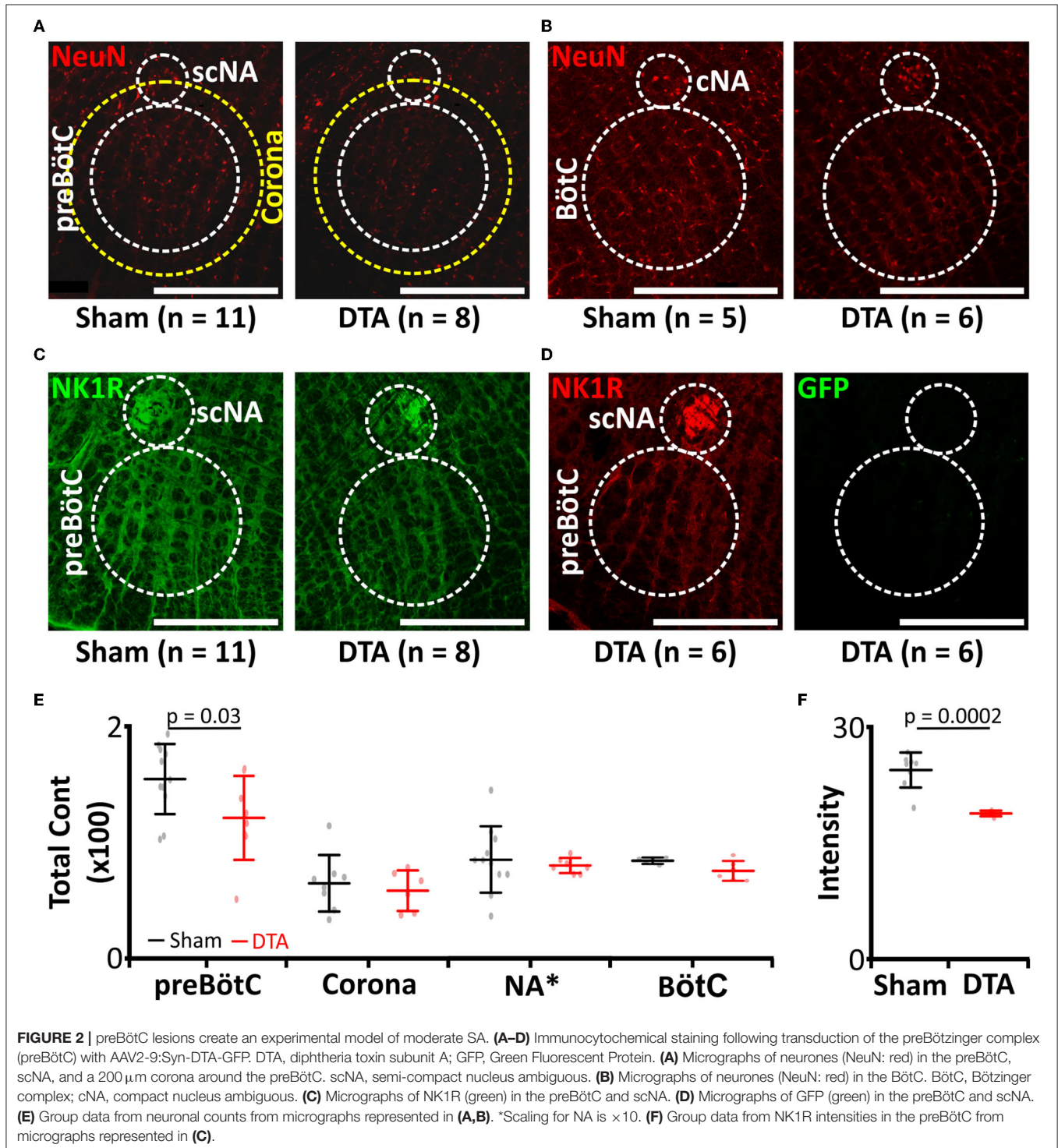
RESULTS

AAV:Syn-DTA (DTA) Transduction of the preBötC Leads to a Lesion of Rhythm-Generating Neurones

Previously, substance-P conjugated to saporin (SP-SAP) was used to induce progressive loss of neurokinin 1 receptor-positive neurones (Mckay and Feldman, 2008). When SP-SAP is injected unilaterally into the inspiratory oscillator, the preBötzing complex (preBötC), it induces SA once the size of lesion reaches \sim 25% of NK1R neurones (Mckay and Feldman, 2008). However, following apoptosis of the neurones, SP-SAP is released back into the extracellular milieu to be taken up by neighbouring neurones that express NK1R. Therefore, the lesion spreads beyond the confines of the preBötC and into the surrounding tissue including the NA [refer to Figure 5 in McKay and Feldman (2008)]. We, therefore, took a different approach to create a stable unilateral partial lesion of the preBötC by stereotaxically targeted viral transduction of the preBötC with an adeno-associated virus (AAV), leading to expression of diphtheria toxin subunit-A (DTA; Figures 1A, 2A–F). Following apoptosis, DTA cannot enter neighbouring cells in the absence of the B subunit (Zalman and Wisniewski, 1984). This creates a stable lesion limited only to the transduced cells. This approach led to a 23% loss of neurones (sham: $1,695 \pm 446$ neurones, $n = 11$ vs. DTA: $1,240 \pm 391$ neurones, $n = 8$; $p = 0.03$; Figures 2A,E). This represented the loss of a significant portion of rhythm-generating cells (sham: 24.4 ± 2.3 NK1R intensity, $n = 8$ vs. DTA: 18.8

± 0.4 NK1R intensity, $n = 5$; $p = 0.0002$; **Figures 2C,F**). DTA inhibits protein synthesis (Strauss and Hendee, 1959), and even a single molecule is enough to induce apoptosis (Yamaizumi et al., 1978). We found rats transduced with the DTA virus displayed no GFP expression ($n = 4$), even though preBötC neuronal numbers were reduced. Therefore, all neurones that expressed

the virus underwent apoptosis. Viral injections were limited to the preBötC, as we saw no loss of neurones in: a 200- μ m corona surrounding the preBötC (sham: 65 ± 24 average number of neurones per slice, $n = 8$ vs. DTA: 58 ± 17 average number of neurones per slice, $n = 6$; **Figures 2A,E**), the NA (sham: 13 ± 2 average number of neurones per slice, $n = 11$ vs. DTA: 12 ± 0

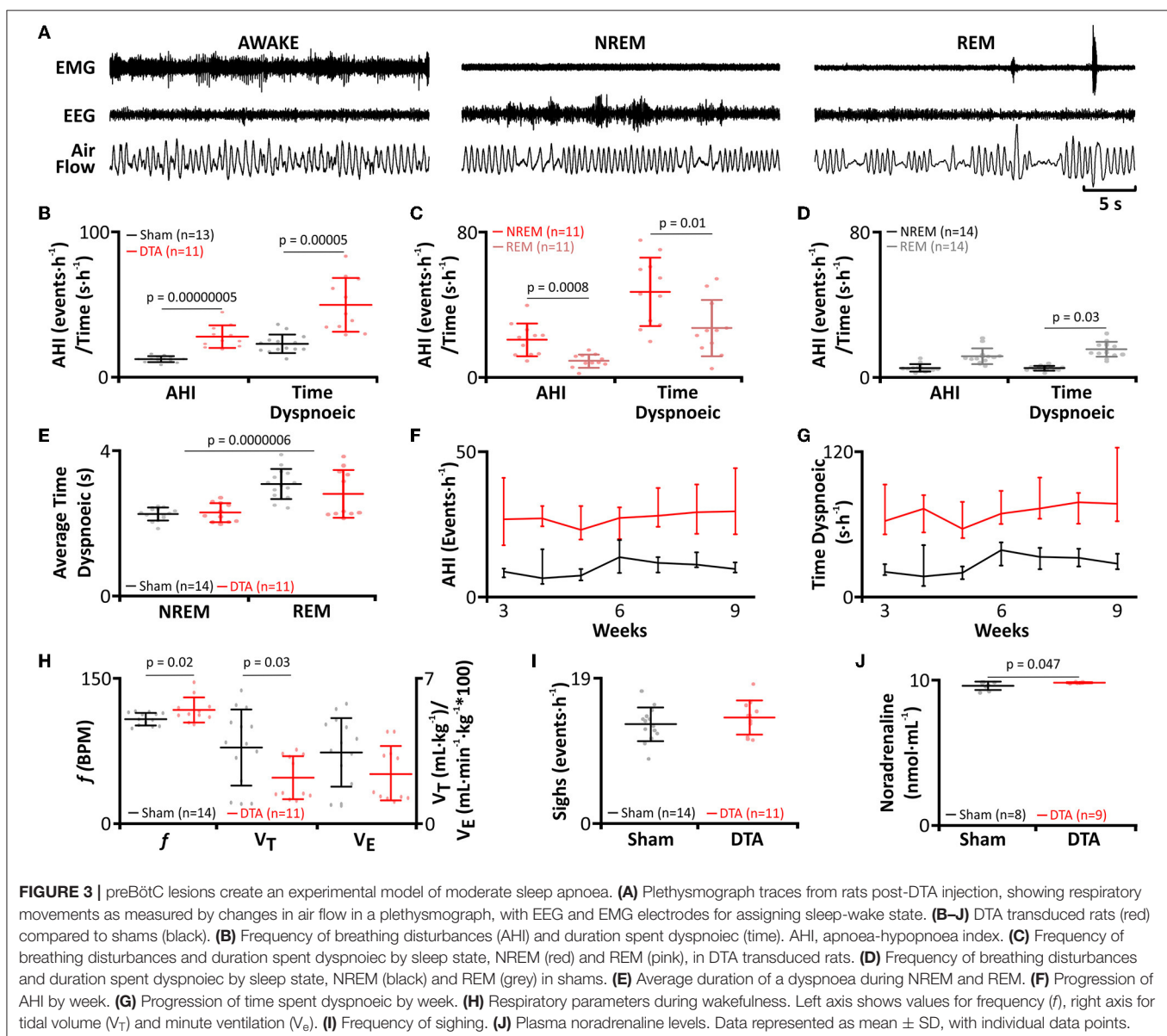


average number of neurones per slice, $n = 7$; **Figures 2A,E**), or the BötC (sham: 83 ± 3 average number of neurones per slice, $n = 5$ vs. DTA: 75 ± 9 average number of neurones per slice, $n = 6$; **Figures 2B,E**).

DTA Lesions Lead to Sleep Disordered Breathing and Alterations in Respiration During Wakefulness

As viral transduction caused a significant lesion of the preBötC, we next studied how this affected breathing and whether this led to SA. Breathing of rats was measured by plethysmography (**Figures 1C, 3A–J**) and sleep-wake state via EEG/EMG recordings (**Figures 1C, 3A**). For assessment of SA severity, we measured the apnoea-hypopnoea index (AHI: sum of apnoeic + hypopnoeic events per hour of sleep), as is done

clinically. A respiratory disturbance was defined as a reduction in minute ventilation of >1.8 s. The AHI was increased in DTA-injected rats (sham: 9 ± 3 incidences-hour of sleep⁻¹, $n = 14$ vs. DTA: 30 ± 9 incidences-hour of sleep⁻¹, $n = 11$; $p = 0.00000005$; **Figure 3B**), as was the total duration of dyspnoeic breathing (apnoeas + hypopnoeas) (sham: 26 ± 6 s, $n = 14$ vs. DTA: 74 ± 25 s, $n = 11$; $p = 0.00005$; **Figure 3B**). Disturbances in the DTA-transduced rats occurred during: 1) NREM sleep (21 ± 9 incidences-hour of sleep⁻¹; 47 ± 7 s-hour of sleep⁻¹; $n = 11$; **Figure 3C**) and REM sleep (9 ± 4 incidences-hour of sleep⁻¹; 27 ± 6 s-hour of sleep⁻¹; $n = 11$; **Figure 3C**). Therefore, NREM contributed a greater number ($\sim 70\%$) of breathing disturbances during sleep ($p = 0.0008$; **Figure 3C**), and a greater time spent dyspnoeic ($p = 0.01$; **Figure 3C**). The number of AHI events did not differ during sleep state in sham-operated rats (NREM: 5 ± 2



incidences·hour of sleep⁻¹, $n = 14$ vs. REM: 5 ± 1 incidence·hour of sleep⁻¹, $n = 14$; **Figure 3D**), although duration was increased in REM (NREM: 12 ± 4 s·hour of sleep⁻¹, $n = 14$ vs. REM: 15 ± 4 s·hour of sleep⁻¹, $n = 14$; $p = 0.03$; **Figure 3D**). The increase in time spent dyspnoeic in REM was due to an increase in duration of the average dyspnoeic event in this sleep state (NREM: 2.3 ± 0.2 s, $n = 25$ vs. REM: 2.9 ± 0.5 s, $n = 25$; $p = 0.0000006$; **Figure 3E**). Interestingly, the average duration of a dyspnoeic event was not affected by transduction with DTA (sham: 2.7 ± 0.5 s, $n = 28$ vs. DTA: 2.5 ± 0.5 s, $n = 22$; **Figure 3E**). The lesions created by DTA transduction created a stable phenotype with the number of incidences and time spent in dyspnoea remaining unchanged between weeks 3 and 9 post-surgery in terms of the number of incidences ($p = 0.95$) and duration spent in dyspnoea ($p = 0.74$) (**Table 1**; **Figures 3E,G**).

Rats with preBötC lesions had an increased f (sham: 95 ± 7 breaths·min⁻¹, $n = 14$ vs. DTA: 105 ± 14 breaths·min⁻¹, $n = 11$; $p = 0.02$; **Figure 3H**), with a reciprocal reduction in V_T (sham: 3.6 ± 2 mL·kg⁻¹, $n = 14$ vs. DTA: 2.3 ± 1 mL·kg⁻¹, $n = 11$; $p = 0.03$; **Figure 3H**). Although slight changes in frequency and tidal volume were seen, the overall integrity of the preBötC and, therefore, respiratory output was not diminished given that V_e remained unchanged (sham: 343 ± 163 mL·kg⁻¹·min⁻¹, $n = 14$ vs. DTA: 244 ± 129 mL·kg⁻¹·min⁻¹, $n = 11$; **Figure 3H**), as did sigh rate (Sham: 13 ± 9 incidences·h⁻¹, $n = 14$ vs. DTA: 14 ± 7 incidences·h⁻¹, $n = 11$; **Figure 3I**). Furthermore, we also found our model of sleep apnoea may have also affected the cardiovascular system given rats transduced with DTA displayed increased plasma noradrenaline (sham: 2 ± 0.3 ng·mL⁻¹, $n = 9$ vs. DTA: 2.4

± 0.4 ng·mL⁻¹, $n = 11$; $p = 0.047$; **Figure 3J**), a marker of increased sympathetic output seen in patients with SA (Ziegler et al., 1997).

Rats With Sleep Apnoea Have Reduced REM Sleep With no Effect on Time Spent in NREM

Given the increase in dyspnoea observed during both phases of sleep, and that dyspnoeas can induce microarousals, we tested whether our DTA-injected rats exhibited any alteration in sleeping patterns. DTA lesions led to the onset of sleep disturbances (**Figure 4**). Apnoeas during NREM sleep were not associated with arousals (**Figure 3A**), and correspondingly, there was no effect on the percentage of time spent in NREM sleep (sham: $48 \pm 4\%$, $n = 14$ vs. DTA: $46 \pm 6\%$, $n = 11$; **Figures 4A–C**). In the majority of cases, during REM sleep, arousals were associated with hyperpnoea that followed a series of dyspnoeas (**Figure 3A**), although in some cases arousal were coincident with the termination of an apnoea (not shown). The arousals caused by apnoeic events decreased the time rats spent in REM sleep by 30% (sham: 6 ± 1 breaths·min⁻¹, $n = 14$ vs. DTA: 4 ± 1 breaths·min⁻¹, $n = 11$; $p = 0.003$; **Figures 4A–C**), with all of the lost REM time being spent awake (sham: $46 \pm 5\%$, $n = 14$ vs. DTA: 52 ± 6 breaths·min⁻¹, $n = 11$; $p = 0.01$; **Figures 4A–C**). Whilst the effects of lesions of preBötC neurones on breathing phenotypes, AHI, and sleep architecture have been studied before (McKay and Feldman, 2008), the physiological and neurological consequences of such lesions remain untested, something we wished to address.

Rats With Sleep Apnoea Have Alterations in Systemic Inflammatory Markers and Plasma Catecholamine Levels

Hypercapnic hypoxia induces chronic inflammation (Maniaci et al., 2021) in patients with SA (McNicholas, 2009). Therefore, we measured the levels of inflammatory markers from inferior vena cava blood samples. Our cytokine panel showed rats with SA displayed increased levels of IFN γ , IL-1b, and MIP (**Table 2**; **Figure 5**) with no change in plasma levels of IL-1a, IL-6, TNF α , MCP-1, and RANTES (**Table 2**; **Figure 5**). Thus, this model of SA produces changes in specific inflammatory markers.

Rats With Sleep Apnoea Have Neuroinflammation

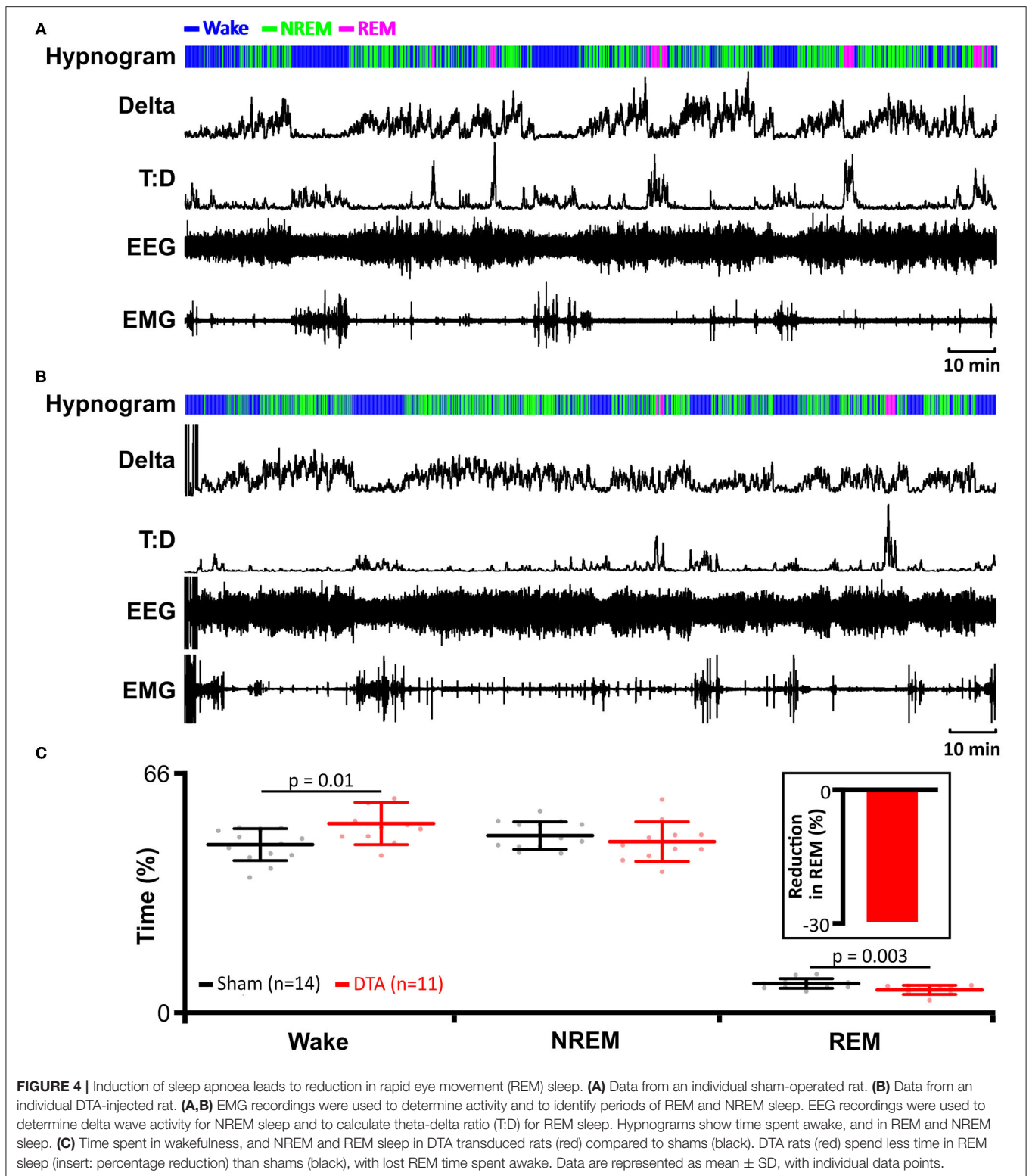
As IL-1b was elevated in SA rats and IL-1b is intimately linked to microglial activation (Monif et al., 2016) and neuroinflammation (Basu et al., 2004), we investigated Iba1 (a marker of activated microglia; Ito et al., 1998) levels in the hippocampus. SA rats displayed neuroinflammation in the hippocampus, which had elevated levels of activated microglia in the CA1 region (sham: $3 R_{70} 20$ cells, $n = 21$ vs. DTA: $21 R_{70} 4$ cells, $n = 7$; $p = 0.007$; **Figures 6A,B**) and dentate gyrus (sham: 5 ± 3 cells, $n = 10$ vs. DTA: 11 ± 3 cells, $n = 7$; $p = 0.001$; **Figures 6C,D**).

TABLE 1 | Apnoea-hypopnoea index (AHI) per hour of sleep of diphtheria toxin fragment A (DTA)-transduced rats by week.

Week	Count	Duration
3	27 R ₇₀ 29	60 R ₇₀ 74
4	27 R ₇₀ 24	72 R ₇₀ 73
5	23 R ₇₀ 35	53 R ₇₀ 79
6	27 R ₇₀ 18	67 R ₇₀ 41
7	27 R ₇₀ 21	72 R ₇₀ 57
8	30 R ₇₀ 25	77 R ₇₀ 65
9	29 R ₇₀ 28	76 R ₇₀ 81

TABLE 2 | Alterations of inflammatory markers in this model of sleep apnoea.

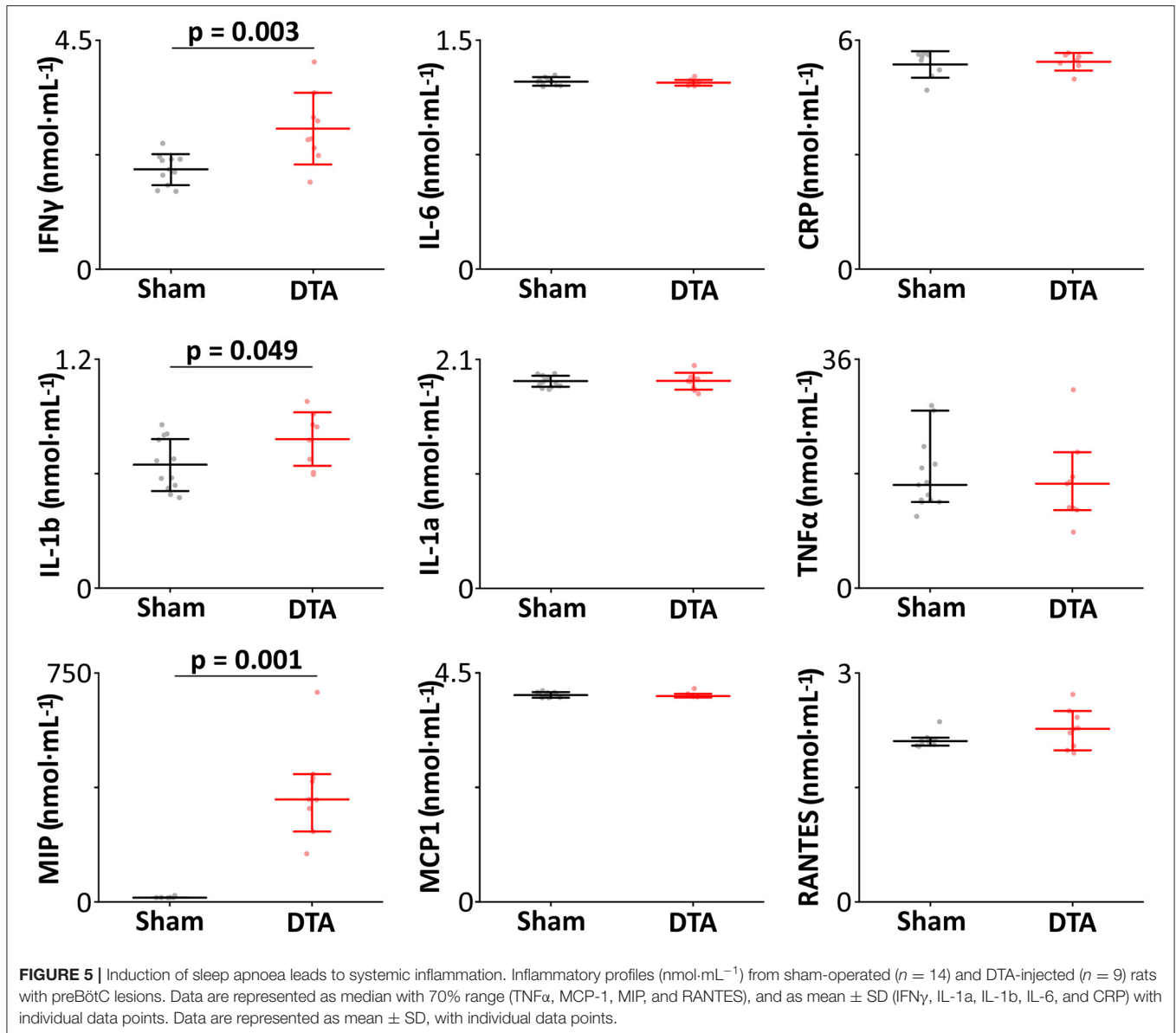
Inflammatory marker	Sham	DTA	Significance
IFN γ	2 ± 0.3 , $n = 11$	2.8 ± 0.7 , $n = 9$	$p = 0.003$
IL-1b	0.6 ± 0.1 , $n = 12$	0.8 ± 0.1 , $n = 8$	$p = 0.049$
MIP	$14 R_{70} 1$, $n = 7$	$336 R_{70} 170$, $n = 9$	$P = 0.001$
IL-1a	1.9 ± 0.1 , $n = 12$	1.9 ± 0.1 , $n = 9$	$p = 0.96$
IL-6	1.2 ± 0.0 , $n = 12$	1.2 ± 0.0 , $n = 8$	$p = 0.6$
TNF- α	$16 R_{70} 9.8$, $n = 13$	$16 R_{70} 8.2$, $n = 9$	$p = 0.5$
MCP-1	$4.0 R_{70} 0.1$, $n = 12$	$4.0 R_{70} 0.1$, $n = 9$	$p = 0.9$
Rantes	$2.1 R_{70} 0.1$, $n = 10$	$2.3 R_{70} 0.5$, $n = 9$	$p = 0.3$



Rats With Sleep Apnoea Have Neurophysiological Changes Resulting in Reduced LTP

We next tested to see if neuroinflammation in SA rats altered the electrophysiological properties in the hippocampus. We first

investigated basal synaptic transmission in the CA1 region of the hippocampus. There was no difference in stimulus input-output curves between SA and sham rats (mean difference $-18.9 \pm 12.2 \text{ mV}\cdot\text{ms}^{-1}$; **Figure 7A**) and in the paired pulse ratio (mean difference 0.0009 ± 0.04 ; **Figure 7B**). Thus, basal



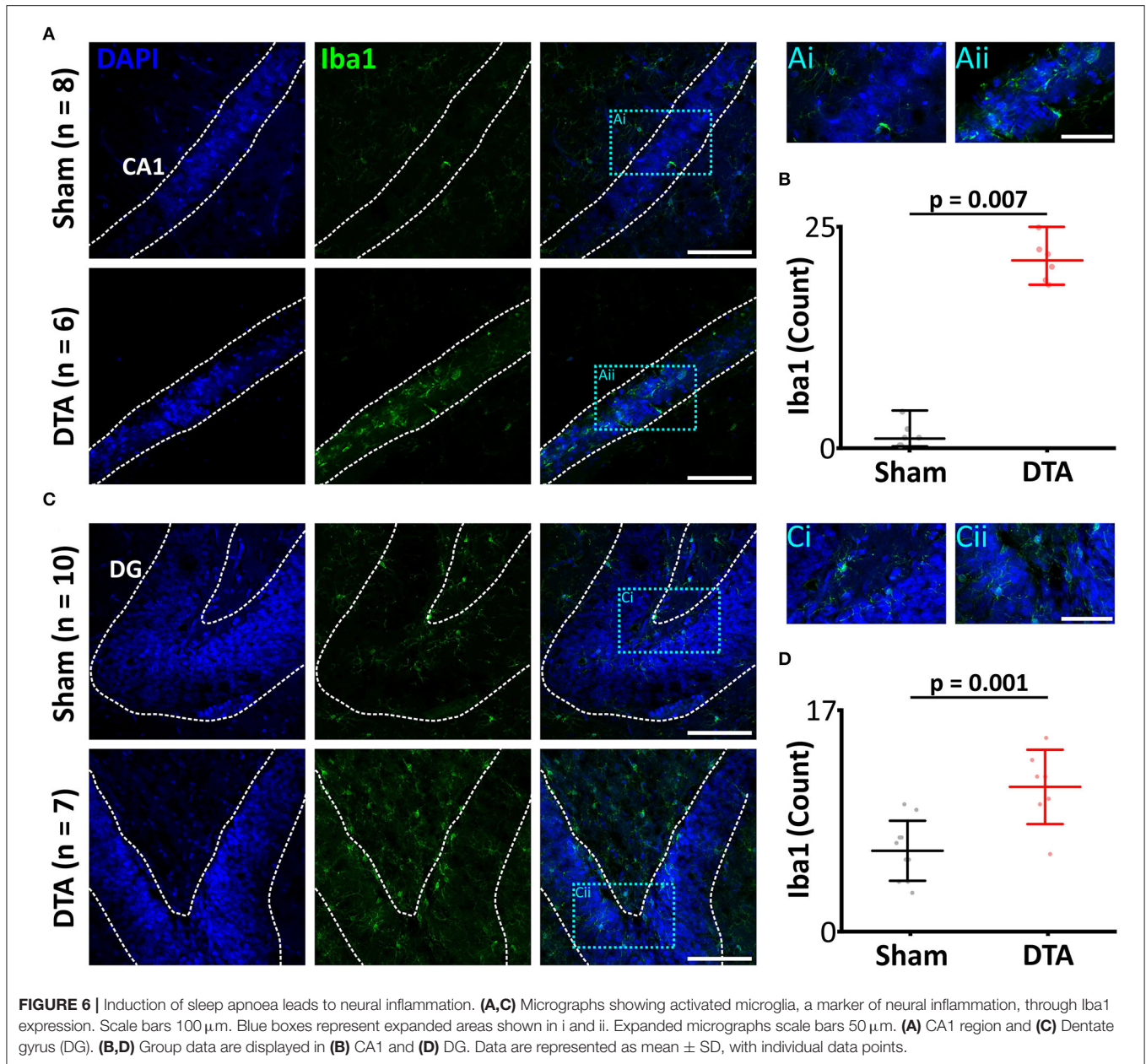
synaptic transmission appears unaffected by sleep apnoea. To investigate long term potentiation (LTP), we used theta burst stimulation (TBS, see methods). SA rats showed decreased LTP following TBS. Both shams (mean difference -0.7 ; standard error 0.1 , $DF = 22$; $p = 0.000005$) and SA rats (mean difference -0.5 ; standard error 0.1 , $DF = 22$; $p = 0.000007$) showed significant short-term potentiation immediately following TBS (Figures 7C,D). However, short-term potentiation was not converted into long-term potentiation in SA rats, as the change in slope was reduced after 1 h (mean difference 0.3 ; standard error 0.1 , $DF = 22$; $p = 0.002$) and was no longer different to baseline (mean difference -0.2 ; standard error 0.1 , $DF = 22$; Figures 7C,D).

In contrast, sham rats displayed LTP, with their change in fEPSP remaining elevated at a level not different to that seen

immediately after TBS (mean difference 0.2 ; standard error 0.1 , $DF = 22$) and higher than baseline (mean difference -0.5 ; standard error 0.1 , $DF = 22$; $p = 0.001$; Figures 7C,D). Overall, SA and sham rats had a similar baseline (mean difference 0.1 ; standard error 0.1 , $DF = 22$) and STP (mean difference 0.2 ; standard error 0.1 , $DF = 22$) fEPSP slopes but not LTP, which was diminished in SA rats (mean difference 0.3 ; standard error 0.1 , $DF = 22$; $p = 0.04$). Thus, SA rats exhibited neurophysiological deficits, which could result in cognitive impairment.

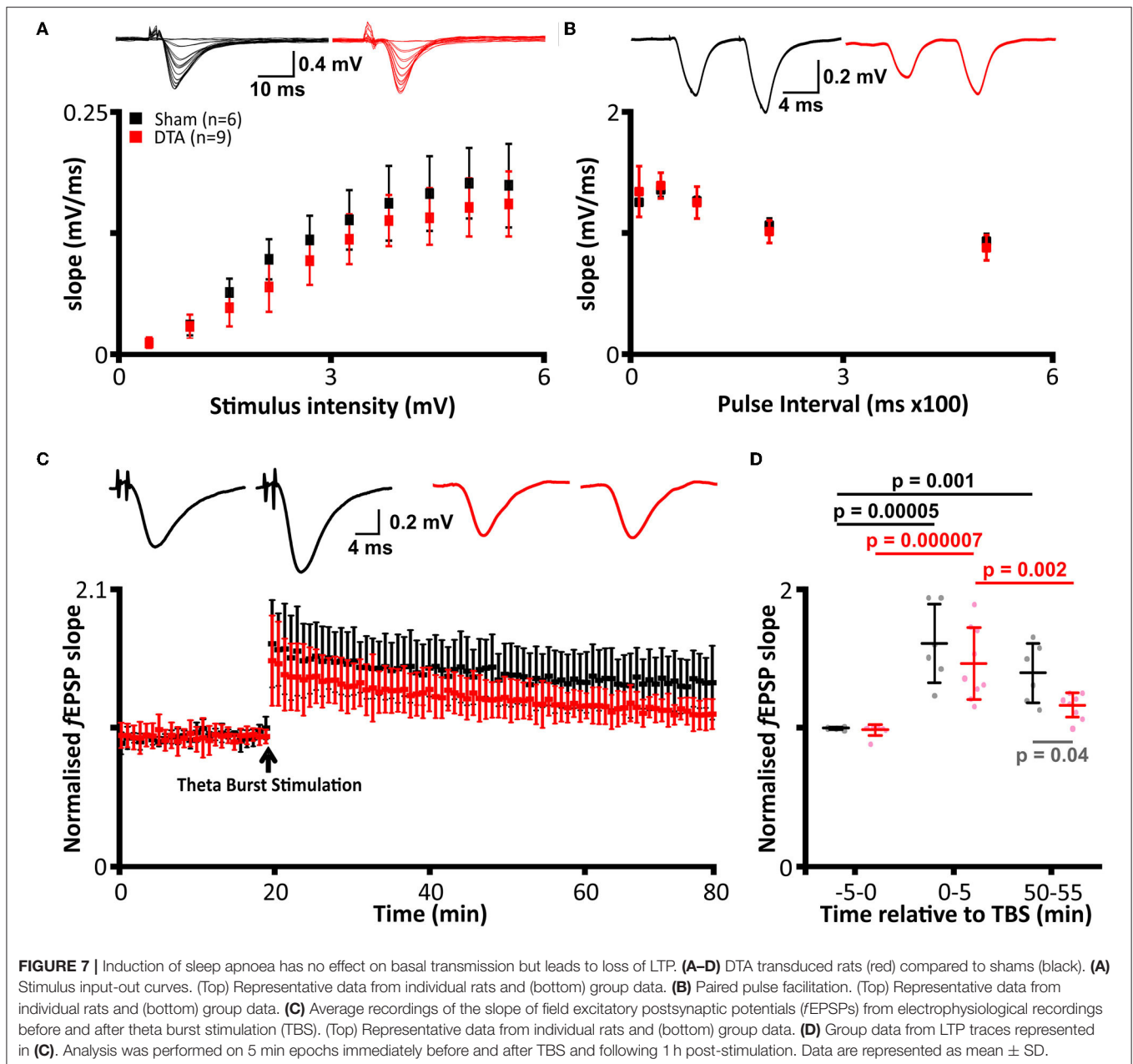
Rats With Sleep Apnoea Have Deficits in Short-Term Memory

Neuroinflammation contributes to cognitive impairment by depletion of synapses and reduction in plasticity (Ma et al., 2014).



We sought to assess how the neuroinflammation we observed in our SA rats affected learning and memory. In a Y-maze forced alteration test (short term memory; tests separated by 1 h), rats with SA displayed no preference for entries into (54% \pm 4%; mean difference 7; standard error 5, DF = 14), duration in (52% \pm 5%, mean difference 4; standard error 6, DF = 13) and distance traveled (53% \pm 4%; mean difference 7; standard error 4, DF = 14) in the novel vs. open arm (**Figures 8A,B**). In contrast, shams displayed a strong preference for the novel arm (entries: 61% \pm 4%, mean difference 22; standard error 6, DF = 14; $p = 0.02$; duration: 57 \pm 5%, mean difference 22; standard error 7, DF = 13; $p = 0.046$; distance traveled: 61 \pm

3%, mean difference 22; standard error 5, DF = 14; $p = 0.004$; **Figures 8A,B**). Interestingly, the discrimination ratio (novel/all arms) showed a decrease in the number of entries (sham: 46% R₇₀ 15%, $n = 4$ vs. DTA: 30% R₇₀ 13%, $n = 9$; $p = 0.03$; data not shown) and distance traveled in the novel arm (sham: 44% R₇₀ 11%, $n = 5$ vs. DTA: 35% R₇₀ 17%, $n = 9$; $p = 0.049$; data not shown) but not the time spent in the novel arm (sham: 31% R₇₀ 14%, $n = 7$ vs. DTA: 32% R₇₀ 11%, $n = 9$; data not shown). The data collected on the Y-maze was not confounded by anxiety or locomotor issues, as rats covered the same distance (sham: 15 \pm 5 m, $n = 7$ vs. DTA: 17 \pm 5 m, $n = 9$; data not shown).



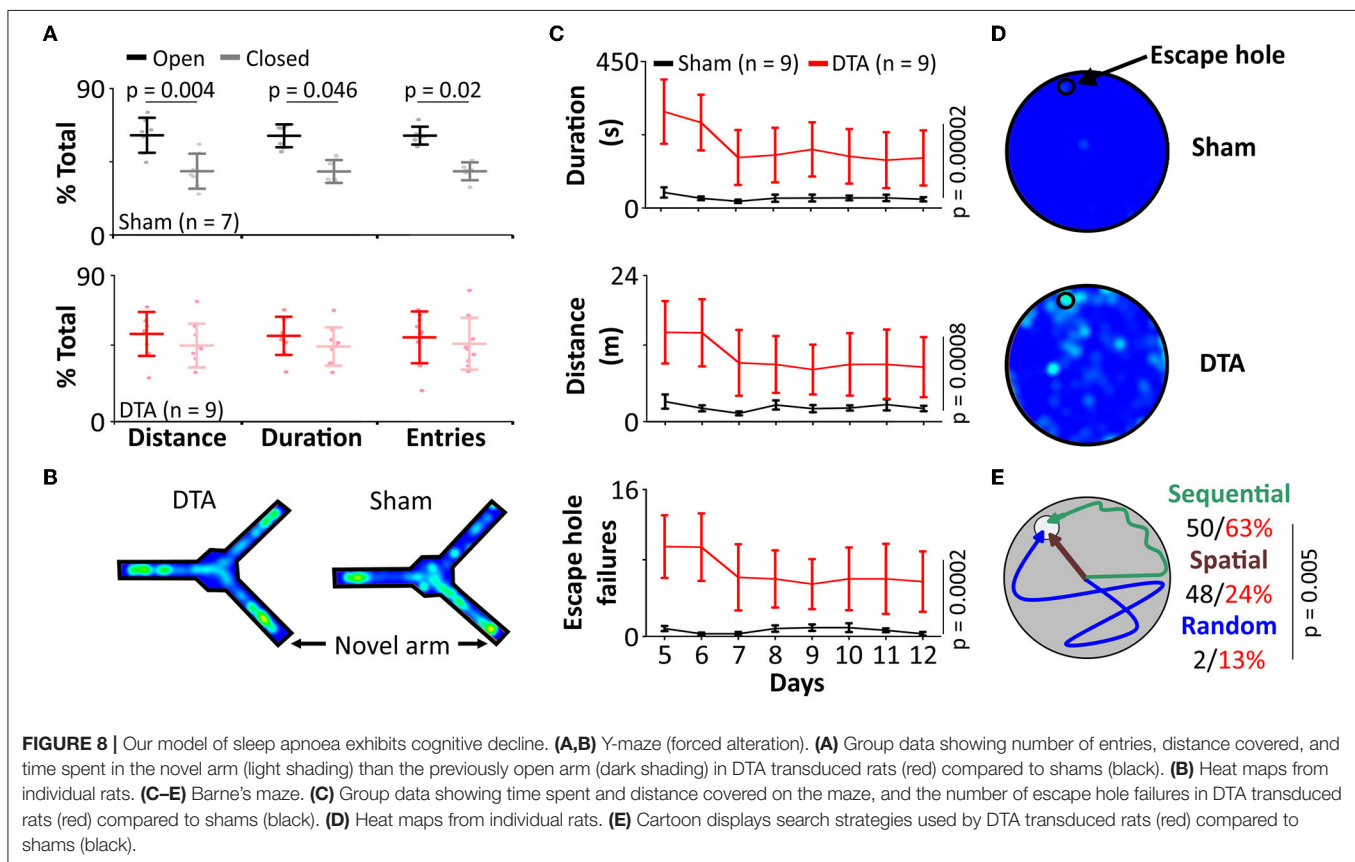
Rats With Sleep Apnoea Have Deficits in Long-Term Memory

As SA rats displayed impaired short-term memory, we next investigated whether they also showed deficits in the conversion of short- to long-term memory. Rats with SA spent longer to find the exit hole in the Barnes maze in terms of duration (sham: 31 ± 25 s vs. DTA: 189 ± 22 s; mean difference 158; standard error 35; DF = 14; $p = 0.00002$) and distance covered (sham: $2.4 \text{ m} \pm 1.5 \text{ m}$ vs. DTA: $10.6 \pm 1.3 \text{ m}$; mean difference -8 ; standard error 2; DF = 14; $p = 0.0008$, **Figures 8C,D**). SA rats failed to use the escape hole more often (sham: 7 ± 1 vs. DTA: 4 ± 2 , mean difference -10 ; standard error 2; DF = 14 $p = 0.0002$;

Figures 8C,D). Furthermore, SA rats were less likely to utilize spatial cues (sham: $48 \pm 17\%$ of trials vs. DTA: $24 \pm 4\%$; of trials $n = 8$ per group; $p = 0.005$) instead preferring a sequential search strategy (64% of trials), with 6 times as many SA rats utilizing a random search strategy (sham: 2% of trials vs. DTA: 13% of trials) (**Figure 8E**).

DISCUSSION

Recently, SA has been gathering attention. Its far-reaching effects as a comorbidity for many diseases makes it a promising target for understanding the mechanisms of those diseases as well as



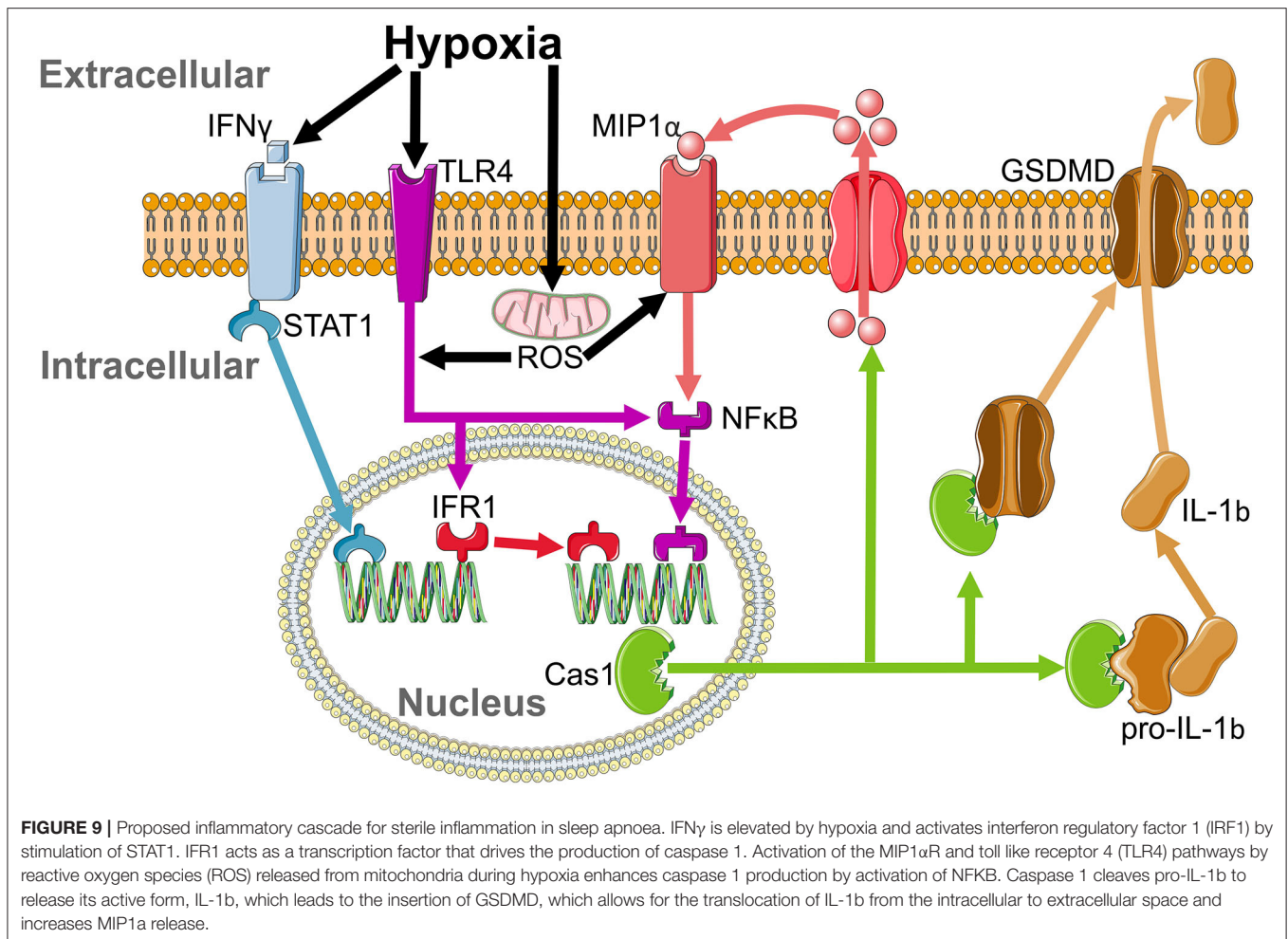
providing new therapeutic targets. The major issue is that until now, there have been no good models for studying SA.

We created a stable lesion of the inspiratory oscillator using a virus to transduce cells to produce the alpha subunit of diphtheria toxin A (DTA). If lesion size is restricted, then loss of respiratory rhythm generating neurones in the preBötC should be compensated for during wakefulness (Mckay and Feldman, 2008). However, during sleep, reduction in chemosensory drive and inhibition of afferent inputs to the respiratory system make breathing more fragile, leading to apnoeas (Mckay and Feldman, 2008). Transduced rats developed sleep disordered breathing that closely resembles the breathing patterns observed in patients with SA.

Whilst we did not record from respiratory muscles, it is likely these apnoeas are central in origin given that obstructive apnoeas are not seen with unilateral ablation of the preBötC (Mckay and Feldman, 2008). Furthermore, arousals in our model were not coincident with the termination of an apnoea, instead arousals were associated with post apnoeic hyperpnoea responsible for reoxygenation; this is indicative of CSA rather than OSA (Jordan et al., 2011; Simms et al., 2013). Nevertheless, as central and obstructive sleep apnoeas can neither be distinguished by oxygen desaturation (Holleboom et al., 2020) nor the sleep state in which they occur (Loadsman and Wilcox, 2000; Gupta et al., 2016), this model constitutes a good representation of both diseases in terms of all but the changes in thoracic pressure seen in OSA.

Furthermore, respiratory changes during wakefulness in rats with SA were similar to the clinical presentation where untreated patients with SA display increased f with reduction in V_T , thus maintaining V_e (Zaremba et al., 2016). Changes in breathing are unlikely to be due to any changes in metabolism, as the preBötC does not project to any nuclei known to be involved in metabolism, with the exception of the lateral hypothalamus (LH) (Tan et al., 2010; Yang and Feldman, 2018). However, only ~50% of neurones in the LH are involved in glucose sensing (Oomura et al., 1969), projections from the preBötC are sparse (Yang and Feldman, 2018), and we only saw a loss of 25% of preBötC neurones, making it unlikely there would be any significant change in metabolism through change in connectivity between the preBötC and LH. Additionally, although respiratory disturbances in SA rats likely lead to changes in blood gases, hypoxia does not cause metabolic changes in middle-aged rats (Haouzi et al., 2009). Finally, minute ventilation is affected by altered metabolism (Huang et al., 1984), whilst there were changes in frequency and tidal volume in SA rats, minute ventilation remains unchanged.

In addition to the respiratory similarities we found, the sleep-wake disturbances in our model mimic the disease. SA patients with and without CPAP showed no change in NREM sleep, but a 26% reduction in REM sleep occurs in patients with untreated SA, with all lost REM time being spent awake (numbers calculated from Table 1 in Aldrich et al., 1989); the same trend we observed in our rats. Alterations in REM sleep are



directly linked to cognitive decline (Moe et al., 1995), and REM sleep disturbances are now thought to be an extremely reliable biomarker for Alzheimer's Disease (AD) (Holth et al., 2017). This sleep deprivation will contribute to a decrease in cognition as REM is crucial for memory consolidation (Boyce et al., 2016), and white matter integrity in older adults (Altendahl et al., 2020). Mechanisms by which REM sleep deprivation causes disruption of learning and memory and changes in the neurophysiology of the hippocampus can include perverse glucose metabolism (Kim et al., 2021), altered neurotransmitter levels (Saygin et al., 2017), inflammation (Yehuda et al., 2009), neuroinflammation (Ashley et al., 2016), and neural damage (Suresh et al., 2021).

Remarkably, we found only a select panel of inflammatory markers elevated in the plasma of our moderate SA model; IFN γ , IL-1b, and MIP. IFN γ activates interferon regulatory factor 1 (IRF1) (Ning et al., 2010) by stimulation of STAT1 (Castro et al., 2018) (Figure 9), with an increase in IRF1 following IFN γ -induced M1 polarization of macrophages (Martinez et al., 2006). IRF1 drives transcription of caspase 1, which cleaves pro-IL-1b to produce the active IL-1b protein (Tsuchiya et al., 2021) (Figure 9). Therefore, modulation of IL-1b is via post-transcriptional modification rather than increased transcription; hence IL-1b protein is increased even though paradoxically its

mRNA is diminished. Caspase 1 further aids IL-1b release by cleaving Gasdermin D (GSDMD) to form the pore responsible for IL-1b release (Tsuchiya et al., 2021) (Figure 9). Once released, IL-1b induces secretion of MIP2 and MIP1 β from parenchymal cells (Rock et al., 2010). In parallel, IFN γ induces both MIP1 α and MIP1 β release from macrophages (Martin and Dorf, 1991), likely in a caspase 1-dependent manner (Liang et al., 2010). This leads us to propose this as a possible mechanism by which moderate SA may affect neural inflammation (Figure 9), and by extension cognition.

Interestingly, whilst IFN γ activation evokes IL-1b and MIP secretion, it cannot by itself induce release of IL-6 (Martin and Dorf, 1991), RANTES (Marfaing-Koka et al., 1995), or MCP-1 (Yamana et al., 2009). Given IL-6 is responsible for inducing CRP release from the liver (Castell et al., 1989), it is therefore not surprising that plasma levels of CRP also remain unchanged. In conjunction, whilst IFN γ -activated macrophages release TNF α (Vila-Del Sol et al., 2008), this is inhibited by hypercapnia (Wang et al., 2010). Hence, TNF α would not be expected to be elevated in response to moderate SA. Finally, cleavage of pro-IL-1 α to IL-1 α occurs through a calpain-dependent, caspase-independent pathway (Tsuchiya et al., 2021). Calpain is inhibited by oxidative stress (Guttmann and Johnson, 1998), while caspase 1 is activated

by it (Kim et al., 2003; Zhang et al., 2003), providing a basis for why IL-1a and IL-1b are differentially regulated during SA.

Hypoxia plays an important role in sterile inflammation. Lowered O₂ increases plasma IFN γ (Roman et al., 2010) and induces toll like receptor 4 (TLR4) (Kim et al., 2010) and MIP1 α receptor (Cowell et al., 2002) upregulation and activation. Increased IFN γ initiates IRF1-dependent inflammation, which is enhanced by hypoxia-induced ROS stimulation of the TLR4 pathway (Dhupar et al., 2011). Furthermore, upregulation of MIP (Kim et al., 2017) and TLR4 (Laghlali et al., 2020) will enhance caspase 1 production by NF κ B activation, amplifying cleavage of pro-IL-1b to its functional form (Kim et al., 2003) and providing a second possible pathway by which hypoxia may lead to neural inflammation (Figure 9). Hence, IFN γ , IRF1, Caspase 1, TLR4, and MIP all drive microgliosis (Kim et al., 2003; Abd-El-Basset et al., 2020). Co-activation of TLR4 and the IFN γ receptor causes significant neuronal dysfunction and cell death (Papageorgiou et al., 2016), with neuronal cell death increased by hypoxia-induced caspase activity (Zhang et al., 2003). Therefore, hypoxia leads to IFN γ -induced microglial activation, which stimulates IRF1 to promote Caspase 1 production to cleave pro-IL-1b, a pathway enhanced by activation of TLR4 and MIP1 α by ROS, leading to microgliosis and neuronal damage (Figure 9). These effects on neural inflammation may be why IFN γ is inversely correlated with cognitive ability (Monteiro et al., 2016) and grey matter volume in the dorsal hippocampus (Monteiro et al., 2016), and may therefore contribute to grey matter loss and mild cognitive impairment (MCI) in patients with SA (Torelli et al., 2011).

Microglial activation induces tau phosphorylation (Yoshiyama et al., 2007) in neurones and promotes conversion of MCI to both Alzheimer's Disease (AD) and Vascular Dementia (VaD) (Olsson et al., 2013). In addition to tau phosphorylation, SA contributes to AD through greater amyloid burden (Bu et al., 2015). SA is independently associated with increased dementia and MCI such as reduced memory or executive function (Sharafkhaneh et al., 2005; Pan and Kastin, 2014), with executive function being more vulnerable than memory, or core intellectual and verbal abilities (Aloia et al., 2004; Saunamäki and Jehkonen, 2007). Accordingly, treatment of SA is able to partially reverse this cognitive decline (Borak et al., 1996; Ooms and Ju, 2016). The loss of REM sleep, the activation of microglia, and the direct effects of inflammation on hippocampal size and function, may be why SA has such profound effects on the brain, and explains the deficits of long and short-term memory we saw in our rats.

Our SA rats display elevated plasma noradrenaline levels, as do patients with SA (Ziegler et al., 1997). Increased catecholamines in plasma are indicative of hypertension, as such patients with SA are at increased risk of dying from cardiovascular events, e.g., heart failure (Gottlieb et al., 2010) and stroke (Redline et al., 2010), which may have an atherosclerotic component (Lui and Ip, 2012) due to systemic inflammation (Libby, 2006; Bosc et al., 2010). Patients with heart failure (HF) treated for OSA have reduced mortality (Javaheri et al., 2011) and morbidity (Lavergne et al., 2015), and every level of HF mortality is directly related to the severity of SA (Lanfranchi et al.,

1999; Lévy et al., 2013). Therefore, this model of SA may also be useful in studying the mechanism linking SA with cardiovascular comorbidities, including VaD, which is elevated in SA patients at higher rates than AD. The severity of cognitive decline in patients with VaD is positively correlated with SA severity (Culebras and Anwar, 2018), with treatment of OSA improving clinical outcomes (Culebras and Anwar, 2018).

In summary, we have developed an improved model of moderate SA that exhibits all of the clinical presentations tested. This model will be a valuable new research tool for investigation of SA directly and as a comorbidity for other disorders such as neurodegeneration.

DATA AVAILABILITY STATEMENT

The authors confirm the data supporting the findings of this study are available in the article, and are available from the corresponding author upon reasonable request.

ETHICS STATEMENT

All experiments involving animals were approved by the University of Warwick Animal Welfare and Ethical Review Board in accordance with the United Kingdom Animals (Scientific Procedures) Act (1986) and the EU Directive 2010/63/EU, and performed under a project license issued by the United Kingdom Home Office.

AUTHOR CONTRIBUTIONS

RR performed experiments and analyzed data from all aspects of the project. MW performed and designed LTP experiments, helped design the Barnes maze experiments, and helped in writing the manuscript. IB designed and made the virus. KD performed plethysmography and ELISAs and analyzed ELISA data. AE performed plethysmography and ELISAs. JD performed plethysmography and Barnes's maze and Y-maze experiments. SN performed immunocytochemistry. RH designed and performed experiments, analyzed data from all aspects of the project, and oversaw the project. All authors commented on the manuscript. All authors contributed to the article and approved the submitted version.

FUNDING

This work was supported by an MRC Discovery Award MC_PC_15070 and Medical and Life Sciences Research Fund bursary.

ACKNOWLEDGMENTS

We would also like to thank Prof. Bruno Frenguelli for allowing the authors to use his equipment and for his consultation during the early designing of the LTP experiments.

REFERENCES

- Abd-El-Basset, E. M., Rao, M. S., and Alsaqobi, A. (2020). Interferon-gamma and interleukin-1beta enhance the secretion of brain-derived neurotrophic factor and promotes the survival of cortical neurons in brain injury. *Neurosci. Insights* 15, 2633105520947081. doi: 10.1177/2633105520947081
- Aldrich, M., Eiser, A., Lee, M., and Shipley, J. E. (1989). Effects of continuous positive airway pressure on phasic events of rem sleep in patients with obstructive sleep apnea. *Sleep* 12, 413–419. doi: 10.1093/sleep/12.5.413
- Aloia, M. S., Arnedt, J. T., Davis, J. D., Riggs, R. L., and Byrd, D. (2004). Neuropsychological sequelae of obstructive sleep apnea-hypopnea syndrome: a critical review. *J. Int. Neuropsychol. Soc.* 10, 772–785. doi: 10.1017/S1355617704105134
- Altendahl, M., Cotter, D. L., Staffaroni, A. M., Wolf, A., Mumford, P., Cobigo, Y., et al. (2020). Rem sleep is associated with white matter integrity in cognitively healthy, older adults. *Plos ONE* 15, E0235395–E0235395. doi: 10.1371/journal.pone.0235395
- Ashley, N. T., Sams, D. W., Brown, A. C., and Dumaine, J. E. (2016). Novel environment influences the effect of paradoxical sleep deprivation upon brain and peripheral cytokine gene expression. *Neurosci. Lett.* 615, 55–59. doi: 10.1016/j.neulet.2016.01.013
- Bahia, C. M. C. D. S., and Pereira, J. S. (2015). Obstructive sleep apnea and neurodegenerative diseases: a bidirectional relation. *Dement. Neuropsychol.* 9, 9–15. doi: 10.1590/S1980-57642015DN9100003
- Basu, A., Krady, J. K., and Levison, S. W. (2004). Interleukin-1: a master regulator of neuroinflammation. *J. Neurosci. Res.* 78, 151–156. doi: 10.1002/jnr.20266
- Borak, J., Cieślowski, J., Koziej, M., Matuszewski, A., and Zieliński, J. (1996). Effects of cpap treatment on psychological status in patients with severe obstructive sleep apnoea. *J. Sleep Res.* 5, 60. doi: 10.1046/j.1365-2869.1996.d01-60.x
- Bosc, L. V. G., Resta, T., Walker, B., and Kanagy, N. L. (2010). Mechanisms of intermittent hypoxia induced hypertension. *J. Cell Mol. Med.* 14, 3–17. doi: 10.1111/j.1582-4934.2009.00929.x
- Boyce, R., Glasgow, S. D., Williams, S., and Adamantidis, A. (2016). Causal evidence for the role of rem sleep theta rhythm in contextual memory consolidation. *Science* 352, 812. doi: 10.1126/science.aad5252
- Brown, D. L., Shafie-Khorassani, F., Kim, S., Chervin, R. D., Case, E., Morgenstern, L. B., et al. (2019). Sleep-disordered breathing is associated with recurrent ischemic stroke. *Stroke* 50, 571–576. doi: 10.1161/STROKEAHA.118.023807
- Bu, X. L., Liu, Y. H., Wang, Q. H., Jiao, S. S., Zeng, F., Yao, X. Q., et al. (2015). Serum amyloid-beta levels are increased in patients with obstructive sleep apnea syndrome. *Sci. Rep.* 5, 13917. doi: 10.1038/srep13917
- Calbet, J. A. L. (2003). Chronic hypoxia increases blood pressure and noradrenaline spillover in healthy humans. *J. Physiol.* 551, 379–386. doi: 10.1113/jphysiol.2003.045112
- Castell, J. V., Gómez-Lechón, M. J., David, M., Andus, T., Geiger, T., Trullenque, R., et al. (1989). Interleukin-6 is the major regulator of acute phase protein synthesis in adult human hepatocytes. *Febs. Lett.* 242, 237–239. doi: 10.1016/0014-5793(89)80476-4
- Castro, F., Cardoso, A. P., Gonçalves, R. M., Serre, K., and Oliveira, M. J. (2018). Interferon-gamma at the crossroads of tumor immune surveillance or evasion. *Front. Immunol.* 9, 847. doi: 10.3389/fimmu.2018.00847
- Chen, H. (2008). Intron Splicing and X2013; mediated expression of aav rep and cap genes and production of aav vectors in insect cells. *Mol. Ther.* 16, 924–930. doi: 10.1038/mt.2008.35
- Chen, Y., Zhong, H., Zhao, Y., Luo, X., and Gao, W. (2020). Role of platelet biomarkers in inflammatory response. *Biomarker Res.* 8, 28. doi: 10.1186/s40364-020-00207-2
- Cowell, R. M., Xu, H., Galasso, J. M., and Silverstein, F. S. (2002). Hypoxic-ischemic injury induces macrophage inflammatory protein-1 α expression in immature rat brain. *Stroke* 33, 795–801. doi: 10.1161/hs0302.103740
- Culebras, A., and Anwar, S. (2018). Sleep apnea is a risk factor for stroke and vascular dementia. *Curr. Neurol. Neurosci. Rep.* 18, 53. doi: 10.1007/s11910-018-0855-1
- Dhupar, R., Klune, J. R., Evankovich, J., Cardinal, J., Zhang, M., Ross, M., et al. (2011). Interferon regulatory factor 1 mediates acetylation and release of high mobility group box 1 from hepatocytes during murine liver ischemia-reperfusion injury. *Shock* 35, 25. doi: 10.1097/SHK.0b013e3181ff6aab0
- Drager, L. F., Polotsky, V. Y., and Lorenzi-Filho, G. (2011). Obstructive sleep apnea: an emerging risk factor for atherosclerosis. *Chest* 140, 534–542. doi: 10.1378/chest.10-2223
- Dusak, A., Ursavas, A., Hakyemez, B., Gokalp, G., Taskapilioglu, O., and Parlak, M. (2013). Correlation between hippocampal volume and excessive daytime sleepiness in obstructive sleep apnea syndrome. *Eur. Rev. Med. Pharmacol. Sci.* 17, 1198–1204.
- Farré, R., Nacher, M., Serrano-Mollar, A., Gáldiz, J. B., Alvarez, F. J., Navajas, D., et al. (2007). Rat model of chronic recurrent airway obstructions to study the sleep apnea syndrome. *Sleep* 30, 930–933. doi: 10.1093/sleep/30.7.930
- Gottlieb, D. J., Yenokyan, G., Newman, A. B., O'connor, G. T., Punjabi, N. M., Quan, S. F., et al. (2010). Prospective study of obstructive sleep apnea and incident coronary heart disease and heart failure: the sleep heart health study. *Circulation* 122, 352–360. doi: 10.1161/CIRCULATIONAHA.109.901801
- Gupta, R., Das, S., Shankar Shilpi, U., Sindhvani, G., and Khandoori, R. (2016). Idiopathic central sleep apnea during rem sleep. *Somnologie* 20, 150–154. doi: 10.1007/s11818-016-0050-z
- Guttmann, R. P., and Johnson, G. V. (1998). Oxidative stress inhibits calpain activity in situ. *J. Biol. Chem.* 273, 13331–13338. doi: 10.1074/jbc.273.21.13331
- Haouzi, P., Bell, H. J., Notet, V., and Bihain, B. (2009). Comparison of the metabolic and ventilatory response to hypoxia and h2s in unsedated mice and rats. *Respir. Physiol. Neurobiol.* 167, 316–322. doi: 10.1016/j.resp.2009.06.006
- Heinzer, R., Vat, S., Marques-Vidal, P., Marti-Soler, H., Andries, D., Tobback, N., et al. (2015). Prevalence of sleep-disordered breathing in the general population: the hypnolaus study. *Lancet Respir. Med.* 3, 310–318. doi: 10.1016/S2213-2600(15)00043-0
- Holleboom, M., Fabius, T., Eijsvogel, M., Van Der Palen, J., and De Jongh, F. (2020). Automatic discrimination between obstructive and central sleep apnea using pulse oximetry. *Eur. Respir. J.* 56, 2115. doi: 10.1183/13993003.congress-2020.2115
- Holth, J. K., Patel, T. K., and Holtzman, D. M. (2017). Sleep in alzheimer's disease—beyond amyloid. *Neurobiol. Sleep Circ. Rhythms* 2, 4–14. doi: 10.1016/j.nbscr.2016.08.002
- Huang, S. Y., Alexander, J. K., Grover, R. F., Maher, J. T., Mccullough, R. E., Mccullough, R. G., et al. (1984). Increased metabolism contributes to increased resting ventilation at high altitude. *Respir. Physiol.* 57, 377–385. doi: 10.1016/0034-5687(84)90085-9
- Ito, D., Imai, Y., Ohsawa, K., Nakajima, K., Fukuuchi, Y., and Kohsaka, S. (1998). Microglia-specific localisation of a novel calcium binding protein, iba1. *Brain Res. Mol. Brain Res.* 57, 1–9. doi: 10.1016/S0169-328X(98)00040-0
- Javaheri, S., Caref, E. B., Chen, E., Tong, K. B., and Abraham, W. T. (2011). Sleep apnea testing and outcomes in a large cohort of medicare beneficiaries with newly diagnosed heart failure. *Am. J. Respir. Crit. Care Med.* 183, 539–546. doi: 10.1164/rccm.201003-0406OC
- Jordan, A. S., Eckert, D. J., Wellman, A., Trinder, J. A., Malhotra, A., and White, D. P. (2011). Termination of respiratory events with and without cortical arousal in obstructive sleep apnea. *Am. J. Respirat. Crit. Care Med.* 184, 1183–1191. doi: 10.1164/rccm.201106-0975OC
- Kim, J. H., Kim, W. S., Hong, J. Y., Ryu, K. J., Kim, S. J., and Park, C. (2017). Epstein-Barr Virus ebna2 directs doxorubicin resistance of b cell lymphoma through ccl3 and ccl4-mediated activation of Nf-kb and btk. *Oncotarget* 8, 5361–5370. doi: 10.18632/oncotarget.14243
- Kim, N. G., Lee, H., Son, E., Kwon, O. Y., Park, J. Y., Park, J. H., et al. (2003). Hypoxic induction of caspase-11/caspase-1/interleukin-1beta in brain microglia. *Brain Res. Mol. Brain Res.* 114, 107–114. doi: 10.1016/S0169-328X(03)00135-9
- Kim, S.-M., Zhang, S., Park, J., Sung, H. J., Tran, T.-D. T., Chung, C., et al. (2021). Rem sleep deprivation impairs learning and memory by decreasing brain o-glcnac cycling in mouse. *Neurotherapeutics* 21, 7. doi: 10.1007/s13311-021-01094-7
- Kim, S. Y., Choi, Y. J., Joung, S. M., Lee, B. H., Jung, Y. S., and Lee, J. Y. (2010). Hypoxic stress up-regulates the expression of toll-like receptor 4 in macrophages via hypoxia-inducible factor. *Immunology* 129, 516–524. doi: 10.1111/j.1365-2567.2009.03203.x
- Laghlali, G., Lawlor, K. E., and Tate, M. D. (2020). Die another way: interplay between influenza a virus, inflammation and cell death. *Viruses* 12, 401. doi: 10.3390/v12040401

- Lanfranchi, P. A., Braghiroli, A., Bosimini, E., Mazzuero, G., Colombo, R., Donner, C. F., et al. (1999). Prognostic value of nocturnal cheyne-stokes respiration in chronic heart failure. *Circulation* 99, 1435. doi: 10.1161/01.CIR.99.11.1435
- Lavergne, F., Morin, L., Armitstead, J., Benjafield, A., Richards, G., and Woehrle, H. (2015). Atrial fibrillation and sleep-disordered breathing. *J. Thorac. Dis.* 7, E575–E584. doi: 10.3978/j.issn.2072-1439.2015.12.57
- Lévy, P., Ryan, S., Oldenburg, O., and Parati, G. (2013). Sleep apnoea and the heart. *Eur. Respir. Rev.* 22, 333. doi: 10.1183/09059180.00004513
- Liang, D.-Y., Li, X., Li, W.-W., Fiorino, D., Qiao, Y., Sahbaie, P., et al. (2010). Caspase-1 modulates incisional sensitization and inflammation. *Anesthesiology* 113, 945–956. doi: 10.1097/ALN.0b013e3181ee2f17
- Libby, P. (2006). Inflammation and cardiovascular disease mechanisms. *Am. J. Clin. Nutr.* 83, 456s–460s. doi: 10.1093/ajcn/83.2.456S
- Loadman, J. A., and Wilcox, I. (2000). Is obstructive sleep apnoea a rapid eye movement-predominant phenomenon? *Br. J. Anaesth.* 85, 354–358. doi: 10.1093/bja/85.3.354
- Lui, M. M.-S., and Ip, M. S.-M. (2012). Osa and atherosclerosis. *J. Thorac Dis* 4, 164–172. doi: 10.3978/j.issn.2072-1439.2012.01.06
- Ma, J., Choi, B.-R., Chung, C., Min, S. S., Jeon, W. K., and Han, J.-S. (2014). Chronic brain inflammation causes a reduction in glun2a and glun2b subunits of nmda receptors and an increase in the phosphorylation of mitogen-activated protein kinases in the hippocampus. *Mol. Brain.* 7, 33. doi: 10.1186/1756-6606-7-33
- Maniaci, A., Iannella, G., Cocuzza, S., Vicini, C., Magliulo, G., Ferlito, S., et al. (2021). Oxidative stress and inflammation biomarker expression in obstructive sleep apnea patients. *J. Clin. Med.* 10, 277. doi: 10.3390/jcm10020277
- Marfaing-Koka, A., Devergne, O., Gorgone, G., Portier, A., Schall, T. J., Galanaud, P., et al. (1995). Regulation of the production of the rantes chemokine by endothelial cells. synergistic induction by ifn-gamma plus tnf-alpha and inhibition by Il-4 And Il-13. *J. Immunol.* 154, 1870–1878.
- Martin, C. A., and Dorf, M. E. (1991). Differential regulation of interleukin-6, macrophage inflammatory protein-1, And Je/Mcp-1 cytokine expression in macrophage cell lines. *Cell Immunol.* 135, 245–258. doi: 10.1016/0008-8749(91)90269-H
- Martinez, F. O., Gordon, S., Locati, M., and Mantovani, A. (2006). Transcriptional profiling of the human monocyte-to-macrophage differentiation and polarization: new molecules and patterns of gene expression. *J. Immunol.* 177, 7303. doi: 10.4049/jimmunol.177.10.7303
- Matuska, P., Kara, T., Homolka, P., and Belehrad, M. (2013). Advances in the management of sleep-disordered breathing in heart failure. *Cor Et Vasa* 55, E411–E418. doi: 10.1016/j.crvasa.2013.06.005
- Mckay, L. C., and Feldman, J. L. (2008). Unilateral ablation of prebotzinger complex disrupts breathing during sleep but not wakefulness. *Am. J. Respir. Crit. Care Med.* 178, 89–95. doi: 10.1164/rccm.200712-1901OC
- McNicholas, W. T. (2009). Obstructive sleep apnea and inflammation. *Prog Cardiovasc Dis* 51, 392–399. doi: 10.1016/j.pcad.2008.10.005
- Moe, K. E., Vitiello, M. V., Larsen, L. H., and Prinz, P. N. (1995). Sleep/wake patterns in alzheimer's disease: relationships with cognition and function. *J. Sleep Res.* 4, 15–20. doi: 10.1111/j.1365-2869.1995.tb00145.x
- Monif, M., Reid, C. A., Powell, K. L., Drummond, K. J., O'brien, T. J., and Williams, D. A. (2016). Interleukin-1 β has trophic effects in microglia and its release is mediated by p2x7r pore. *J. Neuroinflamm.* 13, 173. doi: 10.1186/s12974-016-0621-8
- Monteiro, S., Ferreira, F. M., Pinto, V., Roque, S., Morais, M., De Sá-Calçada, D., et al. (2016). Absence of Ifny promotes hippocampal plasticity and enhances cognitive performance. *Transl. Psychiatry* 6, E707–E707. doi: 10.1038/tp.2015.194
- Ning, Y., Riggins, R. B., Mulla, J. E., Chung, H., Zwart, A., and Clarke, R. (2010). Ifngamma restores breast cancer sensitivity to fulvestrant by regulating stat1, ifn regulatory factor 1, Nf-kappab, Bcl2 family members, and signaling to caspase-dependent apoptosis. *Mol. Cancer Ther.* 9, 1274–1285. doi: 10.1158/1535-7163.MCT-09-1169
- Olsson, B., Hertz, J., Lautner, R., Zetterberg, H., Nägga, K., Höglund, K., et al. (2013). Microglial markers are elevated in the prodromal phase of alzheimer's disease and vascular dementia. *Jad* 33, 45–53. doi: 10.3233/JAD-2012-120787
- Ooms, S., and Ju, Y.-E. (2016). Treatment of sleep disorders in dementia. *Curr. Treat Opt. Neurol* 18, 40–40. doi: 10.1007/s11940-016-0424-3
- Oomura, Y., Ono, T., Ooyama, H., and Wayner, M. J. (1969). Glucose and osmosensitive neurones of the rat hypothalamus. *Nature* 222, 282–284. doi: 10.1038/222282a0
- Pan, W., and Kastin, A. J. (2014). Can sleep apnea cause alzheimer's disease? *Neurosci. Biobehav. Rev.* 47, 656–669. doi: 10.1016/j.neubiorev.2014.10.019
- Papageorgiou, I. E., Lewen, A., Galow, L. V., Cesetti, T., Scheffel, J., Regen, T., et al. (2016). Tlr4-activated microglia require ifn- γ to induce severe neuronal dysfunction and death in situ. *Proc. Natl. Acad. Sci.* 113, 212–217. doi: 10.1073/pnas.1513853113
- Philipps, B., Rotmann, D., Wicki, M., Mayr, L. M., Forstner, M. (2005). Time reduction and process optimization of the baculovirus expression system for more efficient recombinant protein production in insect cells. *Protein Expr Purif.* 42, 211–218. doi: 10.1016/j.pep.2005.03.020
- Poole, S., and Stephenson, J. D. (1977). Body temperature regulation and thermoneutrality in rats. *Q. J. Exp. Physiol. Cogn. Med. Sci.* 62, 143–149. doi: 10.1113/expphysiol.1977.sp002384
- Redline, S., Yenokyan, G., Gottlieb, D. J., Shahar, E., O'connor, G. T., Resnick, H. E., et al. (2010). Obstructive sleep apnea-hypopnea and incident stroke: the sleep heart health study. *Am. J. Respir. Crit. Care Med.* 182, 269–277. doi: 10.1164/rccm.200911-1746OC
- Remmers, J. E., Degroot, W. J., Sauerland, E. K., and Anch, A. M. (1978). Pathogenesis of upper airway occlusion during sleep. *J. Appl. Physiol. Respir. Environ. Exer. Physiol.* 44, 931–938. doi: 10.1152/jappl.1978.44.6.931
- Reutrakul, S., and Mokhlesi, B. (2017). Obstructive sleep apnea and diabetes: a state of the art review. *Chest* 152, 1070–1086. doi: 10.1016/j.chest.2017.05.009
- Rock, K. L., Latz, E., Ontiveros, F., and Kono, H. (2010). The sterile inflammatory response. *Annu. Rev. Immunol.* 28, 321–342. doi: 10.1146/annurev-immunol-030409-101311
- Roman, J., Rangasamy, T., Guo, J., Sugunan, S., Meednu, N., Packirisamy, G., et al. (2010). T-cell activation under hypoxic conditions enhances ifn-gamma secretion. *Am. J. Respir. Cell Mol. Biol.* 42, 123–128. doi: 10.1165/rcmb.2008-0139OC
- Rowley, J. A., Zahn, B. R., Babcock, M. A., and Badr, M. S. (1998). The effect of rapid eye movement (rem) sleep on upper airway mechanics in normal human subjects. *J. Physiol.* 510, 963–976. doi: 10.1111/j.1469-7793.1998.00963.x
- Saunamäki, T., and Jehkonen, M. (2007). A review of executive functions in obstructive sleep apnea syndrome. *Acta. Neurol. Scand.* 115, 1–11. doi: 10.1111/j.1600-0404.2006.00744.x
- Saygin, M., Ozguner, M. F., Onder, O., Doguc, D. K., Ilhan, I., and Peker, Y. (2017). The impact of sleep deprivation on hippocampal-mediated learning and memory in rats. *Bratislavske Lekarske Listy* 118, 408–416. doi: 10.4149/BLL_2017_080
- Sharafkhaneh, A., Giray, N., Richardson, P., Young, T., and Hirshkowitz, M. (2005). Association of psychiatric disorders and sleep apnea in a large cohort. *Sleep* 28, 1405–1411. doi: 10.1093/sleep/28.11.1405
- Simms, T., Brijbassi, M., Montemurro, L. T., and Bradley, T. D. (2013). Differential timing of arousals in obstructive and central sleep apnea in patients with heart failure. *J. Clin. Sleep. Med.* 9, 773–779. doi: 10.5664/jcsm.2918
- Smith, R. H., Levy, J. R., and Kotin, R. M. (2009). A simplified baculovirus-aav expression vector system coupled with one-step affinity purification yields high-titer raav stocks from insect cells. *Mol. Ther.* 17, 1888–1896. doi: 10.1038/mt.2009.128
- Strauss, N., and Hendee, E. D. (1959). The effect of diphtheria toxin on the metabolism of hela cells. *J. Exp. Med.* 109, 145–163. doi: 10.1084/jem.109.2.145
- Suresh, K., Shankar, V., and Cd, D. (2021). Impact of rem sleep deprivation and sleep recovery on circulatory neuroinflammatory markers. *Sleep Sci.* 14, 64–68. doi: 10.5935/1984-0063.20190157
- Tan, A., Cheung, Y. Y., Yin, J., Lim, W.-Y., Tan, L. W. L., and Lee, C.-H. (2016). prevalence of sleep-disordered breathing in a multiethnic asian population in Singapore: a community-based study. *Respirology* 21, 943–950. doi: 10.1111/resp.12747
- Tan, W., Pagliardini, S., Yang, P., Janczewski, W. A., and Feldman, J. L. (2010). Projections of prebotzinger complex neurons in adult rats. *J. Comp. Neurol.* 518, 1862–1878. doi: 10.1002/cne.22308
- Tang, W., Ehrlich, I., Wolff, S. B. E., Michalski, A.-M., Wölfl, S., Hasan, M. T., et al. (2009). Faithful expression of multiple proteins via 2a-peptide self-processing: a versatile and reliable method for manipulating brain circuits. *J. Neurosci.* 29, 8621. doi: 10.1523/JNEUROSCI.0359-09.2009

- Torelli, F., Moscufo, N., Garreffa, G., Placidi, F., Romigi, A., Zannino, S., et al. (2011). Cognitive profile and brain morphological changes in obstructive sleep apnea. *Neuroimage* 54, 787–793. doi: 10.1016/j.neuroimage.2010.09.065
- Tsuchiya, K., Hosojima, S., Hara, H., Kushiyama, H., Mahib, M. R., Kinoshita, T., et al. (2021). Gasdermin D mediates the maturation and release of il-1 α downstream of inflammasomes. *Cell Rep.* 34, 108887. doi: 10.1016/j.celrep.2021.108887
- Veasey, S. C., and Rosen, I. M. (2019). Obstructive sleep apnea in adults. *N. Engl. J. Med.* 380, 1442–1449. doi: 10.1056/NEJMcp1816152
- Vila-Del Sol, V., Punzón, C., and Fresno, M. (2008). Ifn-gamma-induced tnf-alpha expression is regulated by interferon regulatory factors 1 and 8 in mouse macrophages. *J. Immunol.* 181, 4461–4470. doi: 10.4049/jimmunol.181.7.4461
- Wall, M. J., Collins, D. R., Chery, S. L., Allen, Z. D., Pastuzyn, E. D., George, A. J., et al. (2018). The temporal dynamics of arc expression regulate cognitive flexibility. *Neuron* 98, 1124–1132. doi: 10.1016/j.neuron.2018.05.012
- Wang, N., Gates, K. L., Trejo, H., Favoreto, S. Jr., Schleimer, R. P., Sznajder, J. I., et al. (2010). Elevated Co2 selectively inhibits interleukin-6 and tumor necrosis factor expression and decreases phagocytosis in the macrophage. *Faseb J.* 24, 2178–2190. doi: 10.1096/fj.09-136895
- Wasilko, D. J., Lee, S. E., Stutzman-Engwall, K. J., Reitz, B. A., Emmons, T. L., Mathis, K. J., et al. (2009). The titerless infected-cells preservation and scale-up (TIPS) method for large-scale production of NO-sensitive human soluble guanylate cyclase (sGC) from insect cells infected with recombinant baculovirus. *Protein Expr Purif.* 65, 122–132. doi: 10.1016/j.pep.2009.01.002
- Xie, A. (2012). Effect of sleep on breathing—why recurrent apneas are only seen during sleep. *J. Thorac. Dis.* 4, 194–197. doi: 10.3978/issn.2072-1439.2011.04.04
- Yamaizumi, M., Mekada, E., Uchida, T., and Okada, Y. (1978). One molecule of diphtheria toxin fragment a introduced into a cell can kill the cell. *Cell* 15, 245–250. doi: 10.1016/0092-8674(78)90099-5
- Yamana, J., Santos, L., and Morand, E. (2009). Enhanced induction of lps-induced fibroblast mcp-1 by interferon- γ : involvement of jnk and mapk phosphatase-1. *Cell Immunol.* 255, 26–32. doi: 10.1016/j.cellimm.2008.09.003
- Yang, C. F., and Feldman, J. L. (2018). Efferent projections of excitatory and inhibitory prebötzing complex neurons. *J. Comp. Neurol.* 526, 1389–1402. doi: 10.1002/cne.24415
- Yang, Q., Wang, Y., Feng, J., Cao, J., and Chen, B. (2013). Intermittent hypoxia from obstructive sleep apnea may cause neuronal impairment and dysfunction in central nervous system: the potential roles played by microglia. *Neuropsychiatr. Dis. Treat* 9, 1077–1086. doi: 10.2147/NDT.S49868
- Yehuda, S., Sredni, B., Carasso, R. L., and Kenigsbuch-Sredni, D. (2009). Rem sleep deprivation in rats results in inflammation and interleukin-17 elevation. *J. Interferon. Cytokine Res.* 29, 393–398. doi: 10.1089/jir.2008.0080
- Yoshiyama, Y., Higuchi, M., Zhang, B., Huang, S. M., Iwata, N., Saido, T. C., et al. (2007). Synapse loss and microglial activation precede tangles in a p301s tauopathy mouse model. *Neuron* 53, 337–351. doi: 10.1016/j.neuron.2007.01.010
- Young, T., Palta, M., Dempsey, J., Skatrud, J., Weber, S., and Badr, S. (1993). The occurrence of sleep-disordered breathing among middle-aged adults. *New Eng. J. Med.* 328, 1230–1235. doi: 10.1056/NEJM199304293281704
- Zalman, L. S., and Wisnieski, B. J. (1984). Mechanism of insertion of diphtheria toxin: peptide entry and pore size determinations. *Proc. Natl. Acad. Sci.* 81, 3341–3345. doi: 10.1073/pnas.81.11.3341
- Zaremba, S., Shin, C. H., Hutter, M. M., Malviya, S. A., Grabitz, S. D., Macdonald, T., et al. (2016). Continuous positive airway pressure mitigates opioid-induced worsening of sleep-disordered breathing early after bariatric surgery. *Anesthesiology* 125, 92–104. doi: 10.1097/ALN.0000000000001160
- Zhang, W. H., Wang, X., Narayanan, M., Zhang, Y., Huo, C., Reed, J. C., et al. (2003). Fundamental role of the rip2/caspase-1 pathway in hypoxia and ischemia-induced neuronal cell death. *Proc. Natl. Acad. Sci.* 100, 16012–16017. doi: 10.1073/pnas.2534856100
- Ziegler, M. G., Nelesen, R., Mills, P., Ancoli-Israel, S., Kennedy, B., and Dimsdale, J. E. (1997). Sleep apnea, norepinephrine-release rate, and daytime hypertension. *Sleep* 20, 224–231. doi: 10.1093/sleep/20.3.224
- Zuliani, G., Cavalieri, M., Galvani, M., Passaro, A., Munari, M. R., Bosi, C., et al. (2008). Markers of endothelial dysfunction in older subjects with late onset alzheimer's disease or vascular dementia. *J. Neurol. Sci.* 272, 164–170. doi: 10.1016/j.jns.2008.05.020

Conflict of Interest: The authors declare that the research was conducted in the absence of any commercial or financial relationships that could be construed as a potential conflict of interest.

Publisher's Note: All claims expressed in this article are solely those of the authors and do not necessarily represent those of their affiliated organizations, or those of the publisher, the editors and the reviewers. Any product that may be evaluated in this article, or claim that may be made by its manufacturer, is not guaranteed or endorsed by the publisher.

Copyright © 2022 Roberts, Wall, Braren, Dhillon, Evans, Dunne, Nyakupinda and Huckstepp. This is an open-access article distributed under the terms of the Creative Commons Attribution License (CC BY). The use, distribution or reproduction in other forums is permitted, provided the original author(s) and the copyright owner(s) are credited and that the original publication in this journal is cited, in accordance with accepted academic practice. No use, distribution or reproduction is permitted which does not comply with these terms.